JETP Letters, Vol. 78, No. 12, 2003, pp. 745–750. Translated from Pis'ma v Zhurnal Éksperimental'noĭ i Teoreticheskoĭ Fiziki, Vol. 78, No. 12, 2003, pp. 1265–1270.

Giant Air Showers: The Problem of Events with $E_0 \geq 10^{20}$ eV

A. V. Glushkov

Institute of Cosmophysical Research and Aeronomy, Yakut Research Center, Siberian Division, Russian Academy of Sciences, pr. Lenina 31, Yakutsk, 677891 Russia

e-mail: a.v.glushkov@ikfia.ysn.ru

Received November 3, 2003

The problem of the "upper edge" of the energy spectrum of giant air showers (GASs) with $E_0 \geq 10^{19}$ eV is considered. The almost complete absence of GASs with the highest energies ($E_0 \geq 10^{20}$ eV) at the Yakutsk array and their considerable number at AGASA are discussed in view of the fact that both arrays have similar basic detectors and similar procedures of data processing are being used. © *2003 MAIK "Nauka/Interperiodica".*

PACS numbers: 96.40.Pq; 96.40.De; 98.70.Sa

1. INTRODUCTION

Even the first observations of extensive air showers (EASs) at the large Volcano Ranch (USA) [1], Haverah Park (England) [2], SUGAR (Sydney University Giant Air Shower Recorder) [3], and Yakutsk [4] arrays revealed giant air showers (GASs) with energies $E_0 \geq 10^{19}$ eV. After the discovery of cosmic microwave background, it was shown that the flux of primary protons and nuclei interacting with this radiation must decrease abruptly for $E_0 > 3 \times 10^{19}$ eV due to the Greisen–Zatsepin–Kuzmin (GZK) cutoff [5, 6]. Observations at various arrays of GASs whose energies are estimated up to ~$(1–3) \times 10^{20}$ eV [7–10] contradict this prediction. To analyze the problem of the "upper edge" of the energy spectrum of GASs, arrays larger than those mentioned above are constructed. The currently operating Akeno Giant Air Shower Array (AGASA) covers an area of about 100 km^2 [11]. Giant arrays covering an area of ~1000–5000 km^2 with detectors spaced 1–1.5 km apart are under design and construction [12, 13].

However, a strong contradiction between measurements of the energy spectrum of primary cosmic rays (PCR) near $E_0 \sim 10^{20}$ eV exists even at present. On the one hand, only one GAS with $E_0 \approx 1.5 \times 10^{20}$ eV has been detected [8] at the Yakutsk array, which has been in continuous operation for more than 30 years (exposure of ≈ 825 km^2 yr ster). On the other hand, 11 events with $E_0 > 10^{20}$ eV have been detected [14] at AGASA, whose exposure is only twice as large (1649 km^2 yr ster). In view of this discrepancy, Watson [15] criticized the procedures of detection and estimation of GAS energy at the Yakutsk array.

Let us again discuss this problem. First, we note that Watson participated in the detection of six GASs with $E_0 \geq 10^{20}$ eV at the Haverah Park Array [7]. However, none of these events remained after the revision of data and the reduction of the energy estimate by about 30% [16]. The recent revision of Fly's Eye and Hires data also reduced the number of GASs detected with $E_0 \geq 10^{20}$ eV from eight to one [17]. Thus, all arrays in the world (except AGASA) reveal a sharp cutoff in the GAS spectrum at $E_0 \approx 10^{20}$ eV.

2. MEASUREMENTS AT THE YAKUTSK ARRAY

Now, we discuss the critical remarks made in [15]. Watson states that one of the basic factors responsible for the underestimation of the number of GASs with $E_0 \geq 10^{20}$ eV is their missing by the master system of the Yakutsk array. This is an erroneous opinion. First, the coincidence time between two scintillation detectors (each 2 m^2 in area) at all stations is equal to 2 μs and not 1.2 μs, as is stated in [15]. Second, the Yakutsk array has quite a dense network of stations, which form equilateral triangles with a side of 500 and 1000 m at the center and on the periphery, respectively. Since 1995, all stations have been situated within a circle of radius 2 km, forming a triangular network with 500-m sides.

Each station, with any two of its neighbors, is included in the master system selecting showers. When detecting a GAS whose axis is within the array perimeter, two or more master triangles are triggered in the majority of cases. Therefore, the axis of such showers is always at a distance of $R \leq 1000$ m near three or four stations with the maximal particle densities.

Figure 1 shows examples of the measured average lateral distribution functions (LDFs) of all charged particles (dark circles) and muons with a threshold energy

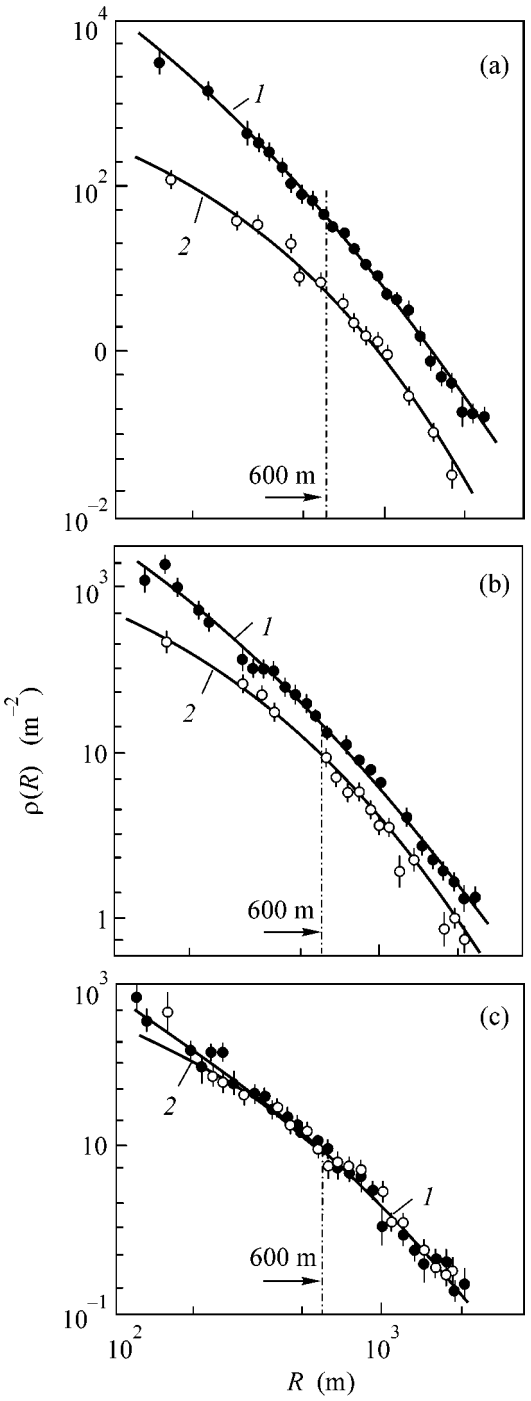

Fig. 1. Lateral distributions of all charged particles (dark circles) and muons (light circles) with threshold energies of $E_\mu \approx 1.0\sec\theta$ GeV in showers with $E_0 = 2 \times 10^{19}$ eV and $\langle\cos\theta\rangle \geq 0.98$ (a), 0.78 (b), and 0.58 (c). Curves *1* and *2* are respective approximations (1) and (2) of the experimental data.

of $E_\mu \geq 1$ GeV (light circles) in GASs with $E_0 = 2 \times 10^{19}$ eV and $\langle\cos\theta\rangle = 0.98$, 0.78, and 0.58 [18]. Solid curves *1* and *2* describe the corresponding approximations

$$f_s(R) = \rho_{s,600}(R/600)^{-1.3} \times ((R + R_M)/(600 + R_M))^{1.3 - b_s} \times ((R + 2000)/2600)^{-3.5} \quad (1)$$

with $b_s = 3.19$, 2.67, and 2.15, and

$$f_\mu(R) = \rho_{\mu,600}(R/600)^{-0.75}((R + 280)/880)^{0.75 - b_\mu} \times ((R + 2000)/2600)^{-8.0} \quad (2)$$

with $b_\mu = 1.92$, 2.07, and 1.32 for three zenith angles, respectively. Here, R_M is the Moliere radius ($R_M = 70$ m for Yakutsk).

It can be seen in Fig. 1a that the density of charged particles in nearly vertical GASs is equal to about 10 m^{-2} at a distance of $R \approx 1000$ m. Therefore, about 20 particles pass through each detector. The probability that two detectors at a station do not display a coincidence over 2 μs is no higher than 10^{-6} for this particle density. In showers with $E_0 \approx 10^{20}$ eV, the particle density at this distance is larger by a factor of about five; i.e., it is equal to about 50 m^{-2}. This circumstance rules out any possibility that the master system of the Yakutsk array does not respond.

Watson [15] states that the second cause for underestimating the number of GASs with $E_0 \geq 10^{20}$ eV at the Yakutsk array is the insufficient time of signal integration by amplitude converters at the stations. In his opinion, this leads to underestimation of the value of $\rho_{s,600}(\theta)$ by about 25%. Accordingly, energy E_0 is underestimated by a factor of 1.25.

This is also an erroneous opinion. The largest GAS was detected at the Yakutsk array at an angle of $\theta = 58.7°$ [8]. It consisted almost completely of muons. The pulse whose shape was measured at the output of one of the standard ground-based scintillation detectors at a distance of $R = 930$ m from the axis had an FWHM of $T_{1/2} \approx 200$ ns. This result agrees with the measurements of the pulse shape at Pierre Auger Observatory [19], where $T_{1/2} \approx 200$ ns was also obtained at the output of the water Cherenkov tank for a GAS with $E_0 \approx (2–3) \times 10^{19}$ eV and $\theta = 54°$ at a distance of $R = 977$ m from the axis. The full width of this signal was equal to about 400 ns. According to the AGASA data [20] and calculations [21], the thickness of the disk for vertical showers at distances $R \approx 1000–2000$ m is about twice as large as that for inclined showers due to the addition of electrons to muons. Hence, it follows that the effective thickness of the disk (95% of all particles) at sea level in a GAS with $E_0 \approx 10^{20}$ eV at a distance of $R \approx 1000$ m from the axis is equal to $T_{0.95} \approx 800$ ns.

We note that analysis of the time structure of the GAS disk at the Haverah Park Array [22] leads to the same conclusion. The Haverah Park and Yakutsk arrays

are situated at approximately the same altitude. Knapp *et al.* [22] measured a time of about 260 ns (for 10 to 50% of the total charge) in a GAS with $E_0 \approx 6 \times 10^{19}$ eV and $\theta = 30°$ at a distance of $R = 1029$ m from the axis. This time corresponds to the effective disk thickness $T_{0.95} \approx 1250$ ns. Therefore, the thickness of the shower disk of all particles in a GAS with $E_0 \approx (2–6) \times 10^{19}$ eV lies in the interval 0.8–1.2 μs (1 μs on the average) at a distance of $R \approx 1000$ m from the axis.

Amplitude signals are measured at the Yakutsk array by using logarithmic *RC* converters (*R* and *C* are the resistance and capacitance of the input circuit, respectively) with a time integration constant of $\tau = RC \approx 10–12$ μs of the input signal *U*,

$$U \sim \exp(-t/\tau). \quad (3)$$

Calculations [23] show that, when ten or more particles fall onto the detector, the input-signal transfer ratio is equal to $k = U/U_0 \approx 1 + d/\tau$ (U_0 is the amplitude of the unperturbed signal and *d* is the half-width of the shower disk). In the case under consideration, $d \approx 0.5$ μs and $k \leq 1.05$. In this case, the density of charged particles is hardly underestimated at distances $R \leq 1000$ m, the more so for measurement of $\rho_{s,\,600}$.

3. MEASUREMENTS AT AGASA

Thus, it has apparently been established that GASs with $E_0 \geq 10^{20}$ eV are virtually absent according to the data from the Yakutsk and other world arrays. In view of this circumstance, let us revise the procedure of determining the energy of a GAS at AGASA. As we previously reported [18, 24–26], showers with $E_0 \geq (3–5) \times 10^{18}$ eV evolve differently than those with lower energies. This statement refers particularly to ultrahigh-energy GASs, whose spatial structure changes significantly.

For a deeper insight into the problem, we compare the LDFs obtained at the Yakutsk array and at AGASA. First, we consider the zenith-angle distributions of parameters $\rho_{s,\,600}(\theta)$ and $\rho_{\mu,\,600}(\theta)$ that are used to estimate energy E_0 at both arrays. These distributions are shown in Fig. 2 for events with $E_0 =$ (a) 2×10^{18}, (b) 10^{19}, and (c) 3×10^{19} eV detected at the Yakutsk array (dark symbols) and AGASA (light symbols). The solid and dashed curves are theoretical LDFs for (*1*) charged particles and (*2*) muons for both arrays. Calculations were carried out in the QGSJET model for primary protons [26]. The Yakutsk data and all calculated values were obtained from average LDFs. Experimental values of $\rho_{s,\,600}(\theta)$ distributions were obtained at AGASA by the method of equal-intensity lines [27], and the $\rho_{\mu,\,600}(\theta)$ distributions for this array refer to muons with a threshold of $E_\mu \approx 1.0 \sec\theta$ GeV [28].

It can be seen that all experimental data for $E_0 = 2 \times 10^{18}$ eV (Fig. 2a) agree with the results of calculations. No such agreement is observed for GASs. The Yakutsk

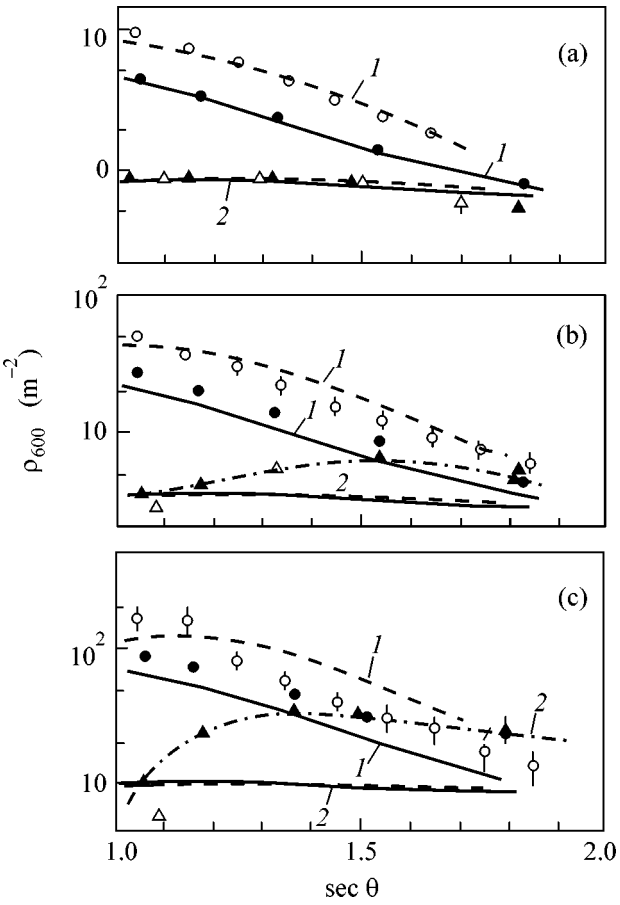

Fig. 2. Parameter ρ_{600} for charged particles (*1*) and muons (*2*) vs. $\sec\theta$ for $E_0 =$ (a) 2×10^{18}, (b) 10^{19}, and (c) 3×10^{19} eV detected at the Yakutsk array (dark symbols) and AGASA (light circles [27] and triangles [28]). The solid and dashed curves are calculated in the QGSJET model for primary protons [26] for the Yakutsk array and AGASA, respectively.

data show that the energies measured for $E_0 = 10^{19}$ eV exceed the calculated values by a factor of ~1.25 (Fig. 2b). Stronger changes are observed for $\rho_{\mu,\,600}(\theta)$ distributions (dot-and-dash curve), which coincide with $\rho_{s,\,600}(\theta)$ for inclined events ($\theta \geq 52°$). In contrast, AGASA data exhibit a tendency to underestimation of the experimental $\rho_{s,\,600}(\theta)$ distributions by a factor of ~1.25 in the zenith-angle range 35°–50°.

The aforementioned anomaly in the development of GASs is enhanced rapidly with an increase in the energy of primary cosmic rays. This is clearly seen in Fig. 2c for showers with $E_0 = 3 \times 10^{19}$ eV. All experimental data completely contradict the predictions of the QGSJET model. This contradiction is not associated with the relatively low statistics of events. The change in the values of $\rho_{\mu,\,600}(\theta)$, which begins to show in the Yakutsk data (dot-and-dash curve *2*), is enhanced further and reaches the triple increase as compared to calculations for $\theta \geq 35°$. Experimental values of $\rho_{s,\,600}(\theta)$

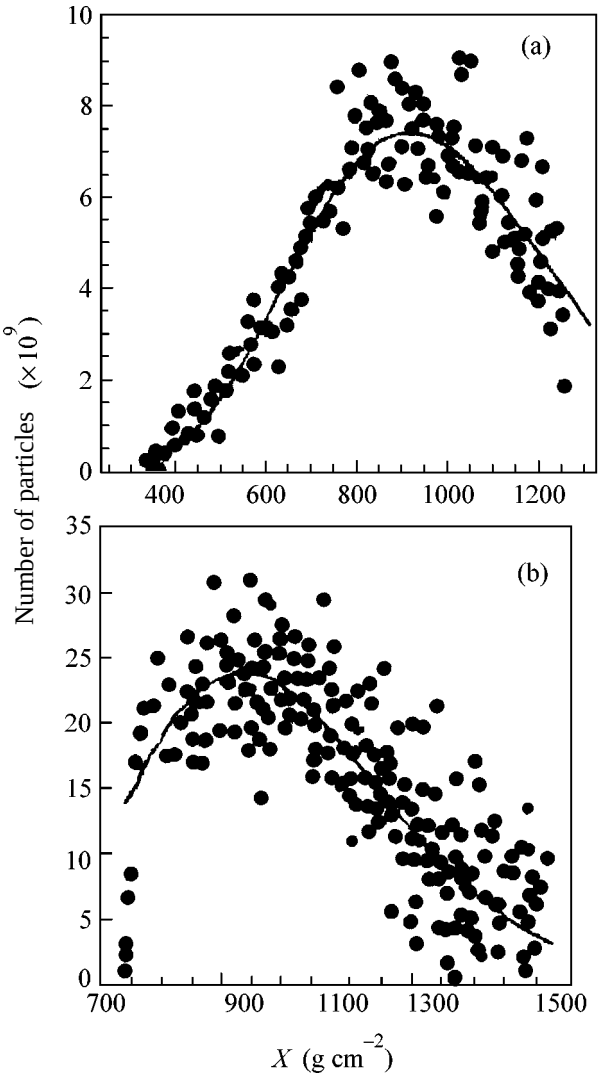

Fig. 3. Cascade curve for GASs with $E_0 = 1.3 \times 10^{19}$ (a) and 3.3×10^{19} eV (b) obtained at the Pierre Auger Observatory [29].

in nearly vertical GASs exceed the calculated values by a factor of ~1.4 and coincide with $\rho_{\mu, 600}(\theta)$ for $\theta \geq 45°$. The AGASA data for $\rho_{s, 600}(\theta)$ in the region of $\theta \leq 30°$ are also larger than the calculated values by a factor of 1.4, decrease rapidly for more inclined showers, are smaller than the results of calculations for $\theta \geq 37°$ by a factor of 1.4, and coincide with the Yakutsk data for $\theta \geq 45°$.

Therefore, only muons with an energy of $E_\mu \geq 1.5$ GeV are detected in these showers at the indicated distance from the axis for $\theta \geq 45°$. There are no softer muons or, the more so, electrons in these showers. The above tendency will apparently be further enhanced when the energy of GASs approaches the limiting value. The disregard of this circumstance probably leads to large errors in estimates of E_0.

Let us now focus special attention on certain important details in Fig. 2c. For $\sec\theta \leq 1.2$, the $\rho_{s, 600}(\theta)$ distributions measured at both arrays are larger than theoretical values by a factor of about 1.5, while the AGASA data for the $\rho_{\mu, 600}(\theta)$ distribution are smaller than theoretical values by a factor of 1.7. For the lateral development of GASs, this can mean that the maximum of the cascade curve is in an anomalously deep position. This assumption is corroborated by the experimental data shown in Fig. 3 for GASs with $E_0 = 1.3 \times 10^{19}$ (a) and 3.3×10^{19} eV (b), which were obtained at the Pierre Auger Observatory [29]. It can be seen that the measured value $X_m \approx 950$ g cm^{-2} is indeed larger than the estimate $X_m \approx 790$ g cm^{-2} in the QGSJET model for primary protons by $\Delta X_m \approx 160$ g cm^{-2}. For AGASA, situated at an altitude of 920 g cm^{-2}, such a situation might be dramatic, because the depth, or maximum, of the development of GASs for $E_0 \approx 10^{20}$ eV lies directly in the array plane (or below it). In this case, to interpret experimental data, it is necessary to use calculations differing from those previously used for EASs with lower energies.

We note one more interesting feature of the data shown in Fig. 2c. It is seen that all experimental $\rho_{s, 600}(\theta)$ distributions measured at the Yakutsk array lie above the calculated curves but are parallel to them. The behavior of the AGASA data (light circles) is different. They intersect theoretical curve *1*. The increase in the values of $\rho_{s, 600}(\theta)$ in nearly vertical GASs (for $\sec\theta \leq 1.2$) with respect to calculations is equal to a factor of about 2.5 as compared to inclined events. The data in Fig. 2a do not show such a feature. This could be a purely methodical experimental error. In the method of equal-intensity lines, which was used to obtain the aforementioned AGASA data, this situation likely appears due to an uncontrolled increase in $\rho_{s, 600}(\theta)$ upon a transition from inclined events to vertical events.

We will show by an example of one of the largest AGASA showers how this can be explained. Dark circles in Fig. 4a show the LDF of charged particles in a GAS with an energy of $E_0 \approx (1.7–2.6) \times 10^{20}$ eV and $\theta \approx 23°$ [30]. The solid curve corresponds to the approximation

$$\rho_s(R) \sim (R/R_M)^{-1.2}(1 + R/R_M)^{1.2-\eta}(1 + (R/1000)^2)^{-0.6} \quad (4)$$

with $R_M = 91.6$ m and with the parameter

$$\eta = 3.97 - 1.79(\sec\theta - 1). \quad (5)$$

This approximation was used to find the coordinates of the shower axis (cross in Fig. 4b). Dark squares are the muon densities with a threshold of $E_\mu \approx 1.0\sec\theta$ GeV. Arrows indicate the saturation of detectors. The atmosphere depth for this event is equal to $X = 920\sec\theta \approx 1000$ g cm^{-2}.

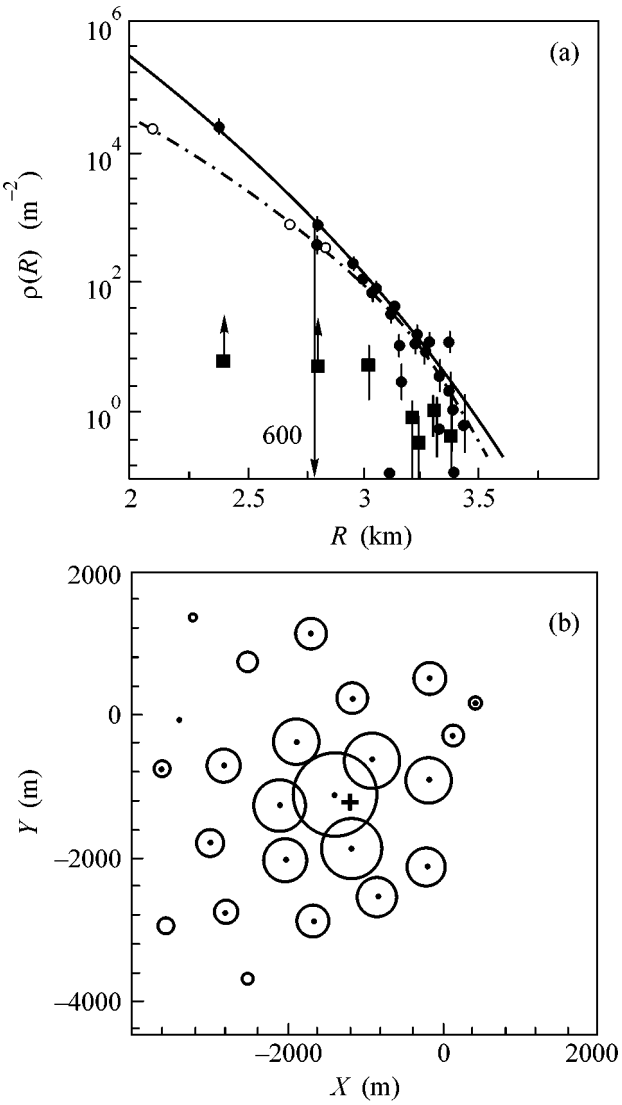

Fig. 4. One of the largest AGASA showers with $E_0 \approx (1.7–2.6) \times 10^{20}$ eV and $\theta \approx 23°$ [30]: (a) LDF of charged particles (dark circles) and muons (dark squares) with threshold $E_\mu \approx 1.0 \sec\theta$ GeV, solid and dot-and-dash curves are approximation (4) and our approximation; (b) density map in the array plan, where the radii of circles are proportional to density logarithm in the corresponding detectors; the cross is the position of the shower axis according to [30].

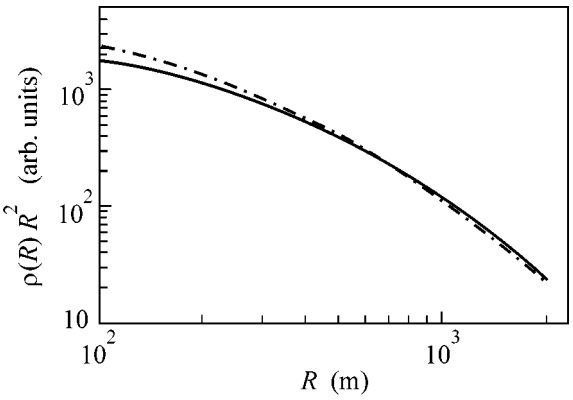

Fig. 5. Lateral distribution function of charged particles in the GAS with $E_0 = 2 \times 10^{19}$ eV at the atmosphere depth X = 1040 g cm^{-2}. Solid curve is approximation (1) with b_s = 3.19, $\cos\theta = 0.98$, and R_M = 91.6 m; dot-and-dash curve is approximation (4) with $\eta = 3.74$ ($\sec\theta = 1.13$).

Let us analyze the results obtained by processing data with another, more convex, LDF (dot-and-dash curve in Fig. 4a). As a result, the GAS axis noticeably approaches the detectors with maximal particle densities: the axis approaches the first and second detectors with the maximal particle numbers (23682 and 687, respectively) by about 120 (light circle) and 100 m, respectively. The axis moves away from the third detector (357 particles) by about 30 m, and the indicated coordinate shift almost does not affect other points in Fig. 4a. This reduces the value of $\rho_{s,600}(\theta) = 892$ m^{-2} obtained at AGASA by a factor of about 2.5. Accordingly; energy E_0 decreases by the same factor.

The dot-and-dash curve in Fig. 4a is just our rough estimate, which is quite possible, however, because the majority of the densities of GASs at AGASA are measured at distances $R > 600$ m. Previously in [18, 26] and in Fig. 2, we showed that the LDFs of charged particles in GASs at the Yakutsk array change substantially. Let us consider the consequence of this fact for AGASA. We use the LDF shown in Fig. 1a (for an atmospheric depth of X = 1040 g cm^{-2}) and replace Moliere radius $R_M = 70$ by 91.6 m in approximation (1). The result is shown by the solid curve in Fig. 5. The dot-and-dash curve in this figure is approximation (4) for the same atmospheric depth (with the parameter $\eta = 3.74$ corresponding to Eq. (5) for $\sec\theta = 1.13 = 1040/920$). Both lines are normalized to each other for R = 1000 m.

It can be seen that the shapes of the LDFs in Fig. 5 are almost undistinguishable for $R \approx 600–2000$ m. This is additional evidence that the measurements of the densities of charged particles at the Yakutsk array at the periphery of GASs are not distorted. However, closer to the axis, approximation (1) is more gently sloping than approximation (4). This tendency is likely enhanced rapidly as the energy of GASs approaches the maximal value. The situation is complicated by the fact that the maximum of the cascade curve is almost at the setup level, where many particles intersect scintillator detectors at distances $R > 1000$ m at very small angles to their surfaces. Under these conditions, the responses of the detectors to particle fluxes can considerably differ from those for much lower energies of EASs.

4. CONCLUSIONS

The above discussion shows that an increase in the number of events with $E_0 \sim 10^{20}$ eV at the operating set-

ups or the construction of setups covering giant areas (1000–5000 km^2) with detectors spaced 1–1.5 km [12, 13] apart cannot help in solving the problem of attainment of maximal energies of GASs. In our opinion, any extrapolation of both theoretical results (obtained for $E_0 \le (2\text{–}3) \times 10^{18}$ eV) and experimental dependences to this region is inadmissible. Such extrapolation can introduce considerable errors in the estimates of the energy of primary particles. In this case, the LDFs of charged particles and muons must be separately investigated at arrays where detectors are spaced no more than 200–300 m apart. Criticism [15] of the methods of detection and estimation of the energy of GASs at the Yakutsk array can hardly be accepted. This criticism is probably due to insufficient popularization of the technical characteristics of the Yakutsk array in the literature.

This study, which is carried out at Yakutsk EAS array, included in the "List of Unique Research and Experimental Setups of National Significance" under no. 01-30, is supported by the Ministry of Education of the Russian Federation.

REFERENCES

1. J. Linsley, Phys. Rev. Lett. **10**, 146 (1963).
2. D. M. Edge, A. C. Evans, H. J. Garmston, *et al.*, J. Phys. A **6**, 1612 (1973).
3. C. J. Bell *et al.*, J. Phys. A **7**, 990 (1974).
4. D. D. Krasilnikov, A. I. Kuzmin, J. Linsley, *et al.*, J. Phys. A **7**, 176 (1974).
5. K. Greisen, Phys. Rev. Lett. **2**, 748 (1966).
6. G. T. Zatsepin and V. A. Kuz'min, Pis'ma Zh. Éksp. Teor. Fiz. **4**, 78 (1966) [JETP Lett. **4**, 53 (1966)].
7. *Catalog of Highest Energy Cosmic Rays Giant Extensive Air Showers* (World Data Center C2 for Cosmic Rays, Japan, 1980), No. 1.
8. N. N. Efimov, T. A. Egorov, A. V. Glushkov, *et al.*, in *Proceedings of International Workshop of Astrophysical Aspects of the Most Energetic Cosmic Rays* (Kofu, 1990), p. 20.
9. N. Hayashida, K. Honda, M. Honda, *et al.*, ICRR Report No. 324-94-19 (Tokyo, 1994).
10. D. J. Bird, S. C. Corbato, H. Y. Dai, *et al.*, Astrophys. J. **424**, 491 (1994).
11. N. Chiba, K. Hashimoto, N. Hayashida, *et al.*, Nucl. Instrum. Methods Phys. Res. A **311**, 338 (1992).
12. J. C. Cronin *et al.*, Preprint EHI 92-08 (Univ. of Chicago, 1992).
13. M. Teshima, M. Bessho, H. Y. Dai, *et al.*, in *Proceedings of RIKEN, International Workshop on Electromagnetic and Nuclear Cascade Phenomena at High and Extremely High Energies* (1993), p. 135.
14. M. Takeda, N. Sakaki, K. Honda, *et al.*, in *Proceedings of 28th ICRC* (Tsukuba, 2003), Vol. 1, p. 381.
15. A. A. Watson, in *Proceedings of 28th ICRC* (Tsukuba, 2003), Vol. 1, p. 373.
16. M. Ave, J. A. Hinton, J. Knapp, *et al.*, in *Proceedings of 27th ICRC* (Hamburg, 2001), Vol. 1, p. 381.
17. T. Abu-Zayyad, G. Archbold, J. A. Bellido, *et al.*, astro-ph/0208243 (2002).
18. A. V. Glushkov, M. I. Pravdin, I. E. Sleptsov, *et al.*, Yad. Fiz. **63**, 1557 (2000) [Phys. At. Nucl. **63**, 1477 (2000)].
19. J. Bluemer *et al.*, in *Proceedings of 28th ICRC* (Tsukuba, 2003), Vol. 1, p. 445.
20. K. Honda, K. Hashimoto, N. Kawasumi, *et al.*, in *Proceedings of 28th ICRC* (Tsukuba, 2003), Vol. 1, p. 361.
21. T. Suomijarvi *et al.*, in *Proceedings of 28th ICRC* (Tsukuba, 2003), Vol. 1, p. 473.
22. M. Ave, J. Knapp, M. Marchesini, *et al.*, in *Proceedings of 28th ICRC* (Tsukuba, 2003), Vol. 1, p. 349.
23. A. N. Gadalov, A. V. Glushkov, T. A. Egorov, *et al.*, in *Experimental Methods for Studying Cosmic Rays of Extremely High Energies* (Yakutsk, 1974), p. 30.
24. A. V. Glushkov, I. T. Makarov, E. S. Nikiforova, *et al.*, Yad. Fiz. **58**, 1265 (1995) [Phys. At. Nucl. **58**, 1186 (1995)].
25. A. V. Glushkov, I. T. Makarov, M. I. Pravdin, *et al.*, Pis'ma Zh. Éksp. Teor. Fiz. **71**, 145 (2000) [JETP Lett. **71**, 97 (2000)].
26. A. V. Glushkov, M. I. Pravdin, I. E. Sleptsov, *et al.*, Yad. Fiz. **65**, 1346 (2002) [Phys. At. Nucl. **65**, 1313 (2002)].
27. M. Nagano, D. Heck, S. Shinozaki, *et al.*, Preprint No. 6191, FZKA (Karlsruhe, 1998).
28. S. Yoshida, N. Hayashida, K. Honda, *et al.*, J. Phys. G **20**, 651 (1994).
29. S. Argiro *et al.*, in *Proceedings of 28th ICRC* (Tsukuba, 2003), Vol. 1, p. 457.
30. N. Hayashida, K. Honda, M. Honda, *et al.*, Phys. Rev. Lett. **73**, 3491 (1994).

Translated by R. Tyapaev

JETP Letters, Vol. 78, No. 12, 2003, pp. 751–756. From Pis'ma v Zhurnal Éksperimental'noĭ i Teoreticheskoĭ Fiziki, Vol. 78, No. 12, 2003, pp. 1271–1276.

Universal Temperature Corrections to the Free Energy for the Gravitational Field¶

G. E. Volovik[1, 2, *] and A. Zelnikov[3, 4]

[1] *Low Temperature Laboratory, Helsinki University of Technology, FIN-02015 HUT, Finland*

[2] *Landau Institute for Theoretical Physics, Russian Academy of Sciences, Moscow, 117334 Russia*

[3] *Theoretical Physics Institute, University of Alberta Edmonton, Alberta, T6G 2J1 Canada*

[4] *Lebedev Physics Institute, Russian Academy of Sciences, Moscow, 119991 Russia*

**e-mail: volovik@boojum.hut.fi*

Received September 15, 2003; in final form, November 10, 2003

The temperature correction to the free energy of the gravitational field is considered which does not depend on the Planck energy physics. The leading correction may be interpreted in terms of the temperature-dependent effective gravitational constant $G_{\rm eff}$. The temperature correction to $G_{\rm eff}^{-1}$ appears to be valid for all temperatures $T \ll E_{\rm Planck}$. It is universal since it is determined only by the number of fermionic and bosonic fields with masses $m \ll T$, does not contain the Planck energy scale $E_{\rm Planck}$ which determines the gravitational constant at $T = 0$, and does not depend on whether or not the gravitational field obeys the Einstein equations. That is why this universal modification of the free energy for gravitational field can be used to study thermodynamics of quantum systems in condensed matter (such as quantum liquids superfluid ^{3}He and ^{4}He), where the effective gravity emerging for fermionic and/or bosonic quasiparticles in the low-energy corner is quite different from the Einstein gravity. © *2003 MAIK "Nauka/Interperiodica"*.

PACS numbers: 04.62.+v; 05.30.-d; 67.90.+z

1. The corrections to the Einstein action for the gravitational field typically depend on the underlying physics of the gravity. There are many ways to produce the gravity: the gravity, of course, can be the fundamental field; but it also can be an effective field induced by quantum fluctuations of massive bosonic or fermionic fields according to the Sakharov scenario [1–3]; it can gradually emerge in the low-energy corner of the fermionic system with massless topologically protected fermions [4]; the metric/vierbein fields can also emerge as a result of the symmetry breaking as a vacuum expectation value of the bilinear combinations of spinor fields [5]; etc. In most cases, the corrections to the Einstein action are nonuniversal since they depend on the trans-Planckian physics. However, there are special cases when the corrections are completely determined by the infrared physics. These corrections are universal since they do not depend on the details of the underlying physics and are the same irrespective of whether the gravity is fundamental or effective. Here, we consider such universal corrections to the free energy for the gravitational field, which come from the infrared fermionic and/or bosonic fields whose masses are small compared to the temperature T.

¶ This article was submitted by the authors in English.

The same universal terms in the free energy for the effective gravity arise in the condensed matter systems, in spite of the fact that the main action, which governs the effective metric, does not resemble the Einstein action even remotely. We discuss such subdominating terms in the bosonic superfluid ^{4}He and fermionic superfluid ^{3}He, where the effective metric field emerges for the bosonic and fermionic quasiparticles, respectively. Since the temperature in these liquids is not very small compared to the corresponding "Planck" scale $E_{\rm Planck}$ (which is typically the Debye temperature or the temperature of superfluid transition T_c), the effect of these terms is accessible for experiments. This allows us to experimentally verify many issues of the interplay of the gravity and thermodynamics.

2. Contribution of massless fermions. *2.1. Relativistic theory.* Let us start with the modification of the free energy for gravity, which comes from the massless fermions. Here, we are interested in the contribution, which comes from the thermal relativistic fermions in the background of the curved space. The free energy of the relativistic gas of fermions in the stationary gravitational field has the correction containing the Ricci curvature $\mathcal{R}$ of the gravitational field. If the gas is in the global equilibrium with temperature T_0 at infinity, one

obtains in the high-temperature limit $T^2 \gg \hbar^2\mathcal{R}$ (but $T \ll E_{\rm Planck}$) the following free energy [6, 8, 9]:

$$F = F_0 - \frac{7\pi^2 N_F}{360\hbar^3}\int d^3x\sqrt{-g}T^4 + \frac{N_F}{288\hbar}\int d^3x\sqrt{-g}T^2[\mathcal{R} + 6w^2]. \quad (1)$$

Here, F_0 is the temperature-independent bulk part of the free energy of a static gravitational field[1]

$$F_0 = -\frac{1}{16\pi G}\int d^3x\sqrt{-g}\mathcal{R}. \quad (2)$$

The T^4 term in Eq. (1), F_4, is the thermal free energy of massless chiral fermions, where N_F is the number of different fermionic species (alternatively, $N_F = 2N_D$ for N_D Dirac fermions with masses $m \ll T$). The temperature T is a local (red-shifted) temperature obeying the Tolman's law

$$T(\mathbf{r}) = \frac{T_0}{\sqrt{|g_{00}(\mathbf{r})|}}, \quad (3)$$

and $T_0 = \text{const}$.

The mixed thermal-gravitational T^2 term F_2 in Eq. (1) is the subject of our discussion. Here, $w^2 = w^\mu w_\mu$, where $w_\mu = \frac{1}{2}\partial_\mu \ln|g_{00}(\mathbf{r})|$ is the 4 acceleration. The temperature-dependent part of the free energy, $F_2 + F_4$, is invariant under stationary conformal transformations [6]. This is because the thermodynamics is determined by the (quasi)particle spectrum, and in the static spacetimes, the energy spectrum $E^2 = -p_i p_k g^{ik}/g^{00}$ does not depend on the conformal factor. The $6w^2$ term in Eq. (1) provides the conformal invariance of the F_2 term.

The total free energy can be represented in terms of the effective gravitational "constant" $G_{\rm eff}$

$$F = -\frac{7\pi^2 N_F}{360\hbar^3}\int d^3x\sqrt{-g}\left(T^4 - \frac{15}{14\pi^2}T^2w^2\right) - \frac{1}{16\pi}\int d^3x\frac{1}{G_{\rm eff}}\sqrt{-g}\mathcal{R}, \quad (4)$$

which is renormalized due to the gravitational polarization of matter and becomes coordinate-dependent due to Tolman's law (3):

$$G_{\rm eff}^{-1}(\mathbf{r}) - G^{-1}(T=0) = -\frac{\pi N_F}{18\hbar}T^2(\mathbf{r}). \quad (5)$$

Alternatively, one could define $G_{\rm eff}$ as prefactor in front of the curvature terms in the equations obtained by variation of the free energy $\delta F/\delta g^{\mu\nu}(\mathbf{r}) = 0$. However, this dynamical definition of $G_{\rm eff}$ does not make much sense for our problems since the effective metric felt by quasiparticles in condensed matter does not satisfy the Einstein equations anyway. Thermodynamic quantities are more robust in this case. That is why here and below we determine $G_{\rm eff}^{-1}$ as the prefactor in front of the curvature $\mathcal{R}$ in the free energy.

It should be mentioned that Eq. (4) is valid for the static (or stationary) case only, since we discuss the system in a global equilibrium. For the same reason, the $\mathcal{R}T^2$ correction, in spite of its formally generally-covariant appearance, in fact is not generally-covariant, since, in a global equilibrium, the reference frame is fixed. Just for the same reason, the free energy for the gauge field violates the Lorentz invariance as was discussed for the static electromagnetic field in [7].

Variation of the free energy over the stationary metric $g^{\mu\nu}(\mathbf{r})$ gives the equations for the stationary metric fields in a global equilibrium, i.e., at fixed T_0. Because of the temperature corrections to the gravitational "constant," $G_{\rm eff}$ itself depends on the metric element g_{00}. As a result, the obtained equations do not coincide with the classical Einstein equations $G_{\mu\nu} = 8\pi G_{\rm eff}T^{\rm M}_{\mu\nu}$, where $G_{\mu\nu}$ is the Einstein tensor and $T^{\rm M}_{\mu\nu}$ is the energy-momentum tensor of matter. Instead, one has

$$G_{\mu\nu} = 8\pi G(T^{\rm M}_{\mu\nu} + T^{\rm M+G}_{\mu\nu}), \quad (6)$$

where $T^{\rm M+G}_{\mu\nu}$ is noncovariant mixed thermal–gravitational term which depends both on the temperature T_0 and on derivatives of the metric tensor. This means that the gravity in a medium is different from the gravity in the vacuum: the matter (here, the relativistic massless fermions at given T_0) is not only the source of gravity but also modifies the gravitational interactions, which depend on the reference frame in which the global equilibrium is achieved.

For us, it is important that the mixed thermal–gravitational term F_2 in the free energy and, thus, the temperature correction to the effective gravitational constant in Eq. (5) are the properties of the low-energy physics of the massless fields in the classical gravitational background: the T^2 correction is universal and does not depend on the physics at Planck scale. It is determined only by the number and type of massless fields which

[1] The main bulk contribution to F_0 comes from the space integral of the Einstein Lagrangian taken with the minus sign [9]. This follows from the relation of the free energy to the Euclidean action $F = TI_{\rm Eucl}$ [10] and the definition of the Euclidean Einstein action $-\frac{1}{16\pi G}\int d^4x\sqrt{g}\mathcal{R}$ with the overall minus sign compare to the Einstein action in Minkowskian signature [11].

are present in the Universe at given temperature, and these fields may have nothing to do with the underlying quantum fields whose vacuum fluctuations contribute to the gravitational constant G at $T = 0$ in induced gravity. This means that the temperature correction does not know whether the gravity is fundamental or effective.

The effect of the polarization of matter in the gravitational field is extremely small in normal conditions, since the temperature is extremely small compared to the Planck energy scale. The renormalization may become important only when $g_{00} \longrightarrow 0$, i.e., when the system is close to the threshold of formation of the horizon or ergoregion. However, in condensed matter, the temperatures are typically not very low compared with the analogs of the Planck energy: the Debye temperature $T_{\rm Debye} \sim 10$ K in superfluid ^{4}He; the superfluid transition temperature $T_c \sim 1$ mK in ^{3}He-A; and the transition temperature $T_c \sim$ 10–100 K in superconductors. That is why this effect can be pronounced in the effective gravity arising in condensed matter.

Moreover, when the thermodynamics or kinetic properties of a condensed matter system are measured, such as the specific heat, entropy, or heat conductivity, the $T = 0$ contribution drops out and the temperature-dependent terms become dominating. In the high-temperature regime $T^2 \gg \hbar^2\mathcal{R}$, the T^4 term is dominating in thermodynamics. However, the curvature simulated by textures in quantum liquids can be made so strong that the subdominating $T^2\mathcal{R}$ term under discussion becomes comparable to the T^4 term, and in principle even the opposite regime $T^2 \ll \hbar^2\mathcal{R}$ can be reached which is called the texture-dominating regime in condensed matter.

Here, we consider the analogs of the $T^2\mathcal{R}$ term on the example of two condensed matter systems.

2.2. Chiral fermions in ^{3}He-A. Let us start with ^{3}He-A, where the effective metric felt by chiral fermionic quasiparticles living in the vicinity of Fermi points (i.e., in the low-energy corner) is [4]

$$g_{ij} = \frac{1}{c_\parallel^2}\hat{l}^i\hat{l}^j + \frac{1}{c_\perp^2}(\delta^{ij} - \hat{l}^i\hat{l}^j), \qquad g_{00} = -1, \quad \sqrt{-g} = \frac{1}{c_\parallel c_\perp^2}. \tag{7}$$

Here, $\hat{\mathbf{l}}$ is the unit vector showing the axis of the uniaxial orbital anisotropy of the superfluid vacuum; the longitudinal and transverse "speeds of light" are

$$c_\parallel = \frac{p_F}{m^*}, \quad c_\perp = \frac{\Delta_0}{p_F} \ll c_\parallel, \tag{8}$$

where p_F and p_F/m^* are Fermi momentum and Fermi velocity correspondingly and Δ_0 is the gap amplitude. We omitted the nonstatic elements g_{0i} produced by the superfluid velocity field, which will be discussed later for the Bose superfluids, and consider the contribution of only the soft Goldstone degrees of freedom related to the deformation of the unit vector $\hat{\mathbf{l}}$ (called textures in condensed matter). That is why the speeds of light are considered as constants in space, as well as g_{00}, which may be chosen as $g_{00} = -1$. This corresponds to the ultrastatic spacetime in general relativity.

Omitting the total derivatives, one can calculate the integral of the Ricci scalar of the metric in Eq. (7):

$$\int d^3x\sqrt{-g}\mathcal{R} = -\frac{1}{2}\int d^3x c_\parallel c_\perp^2\left(\frac{1}{c_\perp^2} - \frac{1}{c_\parallel^2}\right)^2 \times (\hat{\mathbf{l}}\cdot(\nabla\times\hat{\mathbf{l}}))^2 + \text{surface terms}. \tag{9}$$

Let us consider how the term like that enters the free energy of ^{3}He-A. The gradient expansion of the free energy in terms of the gradients of $\hat{\mathbf{l}}$ field has been elaborated by Cross in the limit $c_\perp \ll c_\parallel$ [12]. At that time, it was not known that the effective gravity for quasiparticles emerges at low energy. But now, when we look at the gradient energy derived by Cross, we find that it contains the twist term, which quadratically depends on T [4]:

$$F_2 = -\frac{1}{288\hbar}\int d^3x\frac{c_\parallel}{c_\perp^2}T^2(\hat{\mathbf{l}}\cdot(\nabla\times\hat{\mathbf{l}}))^2 \equiv \frac{1}{144\hbar}\int d^3x\sqrt{-g}T^2\mathcal{R}. \tag{10}$$

Here, $T = T_0$ since $g_{00} = -1$. The thermal part of the free energy does not contain microscopic (trans-Planckian) parameters and is completely determined by the Planck constant $\hbar$ and by the parameters of the spectrum of fermionic quasiparticles in the low-energy limit when the spectrum becomes "relativistic": $E^2 = g^{ik}p_ip_k = c_\parallel^2(\mathbf{p}\cdot\hat{\mathbf{l}})^2 + c_\perp^2(\mathbf{p}\times\hat{\mathbf{l}})^2$ (here, the momentum $\mathbf{p}$ of quasiparticles is counted from the Fermi point). This term exactly coincides with the temperature correction in Eq. (1) in the limit $c_\perp \ll c_\parallel$, since the number of the massless chiral fermions living in the low-energy corner of ^{3}He-A is $N_F = 2$. This demonstrates the universality of the $T^2\mathcal{R}$-term, i.e., its independence of the trans-Planckian physics, while the term F_0 is essentially determined by the trans-Planckian physics [4].

We discussed the contribution to the effective action, which comes from massless fermions. In ^{3}He-A, there are also analogs of massless photons and gauge bosons; moreover, in the logarithmic approximation, the effective electrodynamics obeys the same metric $g_{\mu\nu}$ as fermionic quasiparticles, and, thus, one could expect the similar contribution of the gauge bosons to $G_{\rm eff}^{-1}$.

However, this contribution has not been found. The reason for that is that, in the effective electrodynamics emerging in ^{3}He-A, the nonrenormalizable nonlogarithmic terms are comparable with the covariant terms containing the logarithmically divergent running coupling [4]. As a result, the speed of light for photons differs from the speed of light for chiral fermions. While $c_\parallel$(gauge bosons) = $c_\parallel$(chiral fermions), the transverse speed of light is essentially bigger: $c_\perp$(gauge bosons) $\gg$ $c_\perp$(chiral fermions). Since, according to Eq. (10), $c_\perp$ is in the denominator, the contribution of the gauge bosons to the $T^2\mathscr{R}$ term is negligible.

The contribution of the scalar fields with their own (acoustic) metric will be discussed further in the paper.

3. Contribution of scalar fields. *3.1. Bosonic field.* The origin of the effective gravity in superfluid ^{4}He is essentially different from that in ^{3}He-A. The superfluid ^{3}He-A belongs to the same universality class of the fermionic systems as the quantum vacuum of the Standard Model, and one can expect that these systems have a common origin of the emerging gravity represented by the collective modes related to the deformation of Fermi points. The superfluid ^{4}He is the Bose liquid where bosonic quasiparticles—phonons—play the role of a scalar field, propagating in the background of the effective metric $g_{\mu\nu}$ provided by the moving superfluid condensate (superfluid quantum vacuum). The gravity field $g_{\mu\nu}$ experienced by phonons is simulated mainly by the superfluid velocity field $\mathbf{v}_s$ (velocity of the superfluid quantum vacuum). The dynamics of the velocity field is determined by the hydrodynamic equations instead of the Einstein equations. Nevertheless, the universal $T^2\mathscr{R}$ term must enter the effective action for $g_{\mu\nu}$, and this term must be universal, as in Eq. (5) but with the prefactor determined now by the number N_s of scalar fields with masses $m \ll T$ [6, 13]:

$$F = F_0 - \frac{\pi^2 N_s}{90\hbar^3}\int d^3x\sqrt{-g}T^4 - \frac{N_s}{144\hbar}\int d^3x\sqrt{-g}T^2[\mathscr{R} + 6w^2]. \tag{11}$$

In general relativity, this leads to the following modification of the effective gravitational constant determined as the prefactor in front of the curvature in the free energy functional:

$$G_{\rm eff}^{-1} - G^{-1}(T=0) = \frac{\pi}{9\hbar}N_s T^2. \tag{12}$$

3.2. Phonon contribution in superfluid ^{4}He. Phonons obey the following effective metric (which is called the acoustic metric [14]):

$$\sqrt{-g} = \frac{1}{c^3}, \quad g_{00} = -\left(1 - \frac{\mathbf{v}_s^2}{c^2}\right), \quad g_{ij} = \frac{1}{c^2}\delta_{ij}, \quad g_{0i} = -\frac{v_{si}}{c^2}, \tag{13}$$

where c is the speed of sound; $\mathbf{v}_s$ is the superfluid velocity; and we neglected the conformal factor which depends on the mass density ρ of the liquid. Let us consider the simplest case when the velocity field is stationary. This means that there is a preferred reference frame, in which the velocity field does not depend on time, and $\mathbf{v}_s(\mathbf{r})$ is the velocity with respect to this frame. The metric is, thus, stationary but not static. Let us also assume for simplicity that c and ρ are space-independent. Then, the expression for curvature in terms of the velocity field is [15]

$$\mathscr{R} = \frac{1}{2}(\nabla\times\mathbf{v}_s)^2 + \nabla\cdot(\mathbf{v}_s(\nabla\cdot\mathbf{v}_s)) + \nabla\cdot((\mathbf{v}_s\cdot\nabla)\mathbf{v}_s). \tag{14}$$

For pure rotation $\mathbf{v}_s = \Omega\times\mathbf{r}$, the curvature is zero $\mathscr{R} = 0$, since this corresponds to Minkowski spacetime in the rotating frame. For this reason, let us consider the case when the velocity of the superfluid vacuum is curl-free ($\nabla\times\mathbf{v}_s = 0$), which is the case for superfluid ^{4}He when quantized vortices are absent. Then, one has

$$\mathscr{R} = \nabla_i\nabla_k(v_{si}v_{sk}). \tag{15}$$

If, in addition, the superfluid vacuum is incompressible ($\nabla\cdot\mathbf{v}_s = 0$), the curvature transforms to

$$\mathscr{R} = \frac{1}{2}\Delta(\mathbf{v}_s^2) = \frac{1}{2}c^2\Delta g_{00} = -\Delta\Phi, \tag{16}$$

where Φ is the analog of the gravitational potential: $g_{00} = -(1 + 2\Phi/c^2)$.

Let us apply Eq. (11) to the superfluid ^{4}He where $N_s = 1$. For simplicity, we consider the static effective spacetimes, i.e., those which satisfy the condition $\nabla\times(\mathbf{v}_s/(c^2 - v_s^2)) = 0$. Then, integrating by parts, one obtains

$$F - F_0 = \int d^3x\left(-\frac{\pi^2T^4}{90\hbar^3c^3} - \frac{T^2}{144\hbar c^5}\frac{\nabla(\mathbf{v}_s^2)\cdot\nabla(\mathbf{v}_s^2)}{1-\mathbf{v}_s^2/c^2}\right). \tag{17}$$

Let us note that $T(\mathbf{r}) = T_0/\sqrt{1-\mathbf{v}_s^2(\mathbf{r})/c^2}$ is a red-shifted temperature measured by the local observer who lives in the liquid and uses phonons for communication,

while T_0 is the real temperature of the liquid, which is constant across the container in a global equilibrium.

Note that the free energy F_0 for the effective gravity itself (the hydrodynamic energy of superfluid ^{4}He in terms of $\mathbf{v}_s$ and ρ) is very different from that in general relativity, and it certainly cannot be represented only in terms of the curvature term $\sqrt{-g}\mathcal{R}$. This is because the hydrodynamic equations being determined by the ultraviolet "Planck-scale" physics are not obeying the effective acoustic metric (13). The same actually occurs in ^{3}He-A, though the effective gravity there is essentially improved as compared to that in superfluid ^{4}He, and one can even identify some of the components of the Einstein action. However, in both liquids, the temperature correction to the curvature term in Eqs. (17) and (10) is within the responsibility of the emerging infrared relativistic physics and is independent of the microscopic (Planck) physics.

3.3. Fields with different effective metrics. In the fermionic liquid, the velocity-dependent $T^2\mathcal{R}$ term (such as the second term in Eq. (17)) is also present. Actually, there are even several such terms: one comes from $N_F = 2$ chiral fermions with their metric $g^F_{\mu\nu}$ in Eq. (7) modified by the superfluid velocity field (see Eq. (9.13) in [4]); another one comes from the massless scalar field of the sound with its acoustic metric $g^s_{\mu\nu}$ in Eq. (13); and there are also two massless scalar fields of spin waves with their own "spin-acoustic" metric. These contributions to the T^2 correction can be combined in the following way:

$$F_2 = \frac{T_0^2}{288\hbar}\int d^3x\left(\sum_F \frac{\sqrt{-g^F}}{|g^F_{00}|}(\mathcal{R}_F + 6w_F^2) - 2\sum_s \frac{\sqrt{-g^s}}{|g^s_{00}|}(\mathcal{R}_s + 6w_s^2)\right). \quad (18)$$

Here, T_0 is the real temperature in the liquid, which is constant in a global equilibrium, while the local redshifted temperature is different for different quasiparticles, since it depends on the effective metric experienced by a given excitation.

4. Discussion. There are many condensed matter systems where the low-energy quasiparticles obey the effective Lorentzian metric. The dynamics of this effective metric is, typically, essentially different from the dynamics of the gravitational field in Einstein theory. However, the thermodynamics appears to be identical, since it is determined solely by the infrared physics, which does not depend on whether the gravity is fundamental or effective. This similarity can be useful both for condensed matter and for gravity.

In particular, this will be useful for the consideration of the low-temperature limit. The procedure of the gradient expansion in quantum liquids assumes that the gradients are smaller than all other quantities; in particular, the correction to the action for the metric field in Eq. (10) is valid only if the effective curvature is small enough: $\hbar^2\mathcal{R} \ll T^2 \ll E^2_{\rm Planck} \equiv \Delta_0^2$, i.e., when the temperature is relatively high. However, in quantum liquids or superconductors, the opposite (texture-dominating) limit $T^2 \ll \hbar^2\mathcal{R} \ll E^2_{\rm Planck}$ is also achievable. Moreover, the thermodynamic effects related to the textures (curvature) become dominating in this limit. An example is provided by the $-T^2\sqrt{\mathcal{B}}$ term in the free energy of the quasi-two-dimensional *d*-wave superconductor in applied magnetic field $\mathcal{B}$ [16]. This term comes from the gapless fermions in the background of the $U(1)$ field, whose curvature $\mathcal{B}$ substitutes the Riemann curvature $\mathcal{R}$ of the gravitational field. It determines the thermodynamics of *d*-wave superconductors in the low-T limit $T^2 \ll \mathcal{B}$, and, in particular, the specific heat $C \propto T\sqrt{\mathcal{B}}$ has been measured in cuprate superconductors [17]. Whether the corresponding gravitational term $-T^2\sqrt{\mathcal{R}}$ appears at $T^2 \ll \hbar^2\mathcal{R}$ in the free energy of quasi-two-dimensional systems with effective Lorentzian metric is the problem for future investigations.

Since these effects are determined solely by the infrared physics, one can use for their calculations the methods developed in the relativistic theory. Since these terms are not sensitive to the dynamics of the effective gravity field, one can assume that this dynamics is governed by the Einstein equations. Then, the powerful theorems derived for the Einstein gravity can be used, including the connection between the curvature terms in the free energy and the entropy of the horizon. Thus, the condensed matter can serve as the arena where the connection between the gravity and thermodynamics can be exploited and developed.

We are grateful to A.A. Starobinsky for numerous discussions. This work was supported by ESF COSLAB Programme and by the Russian Foundation for Basic Research. A.Z. is grateful to the Killam Trust for its financial support.

REFERENCES

1. A. D. Sakharov, Dokl. Akad. Nauk SSSR **177**, 70 (1967) [Sov. Phys. Dokl. **12**, 1040 (1968)]; Gen. Relativ. Gravit. **32**, 365 (2000).
2. T. Jacobson, gr-qc/9404039.
3. V. P. Frolov, D. V. Fursaev, and A. I. Zelnikov, Nucl. Phys. B **486**, 339 (1997).
4. G. E. Volovik, *The Universe in a Helium Droplet* (Clarendon Press, Oxford, 2003).
5. C. Wetterich, hep-th/0307145.
6. Yu. V. Gusev and A. I. Zelnikov, Phys. Rev. D **59**, 024002 (1999).

7. D. V. Fursaev, hep-th/0311080; D. V. Fursaev, Nucl. Phys. B (Proc. Suppl.) **104**, 33 (2002); hep-th/0107089.
8. J. S. Dowker and J. P. Schofield, Nucl. Phys. B **327**, 267 (1989).
9. V. P. Frolov and A. I. Zelnikov, Phys. Rev. D **35**, 3031 (1987).
10. J. W. York, Jr., Phys. Rev. D **33**, 2092 (1986).
11. S. W. Hawking and C. J. Hunter, Class. Quantum Grav. **13**, 2735 (1996).
12. M. C. Cross, J. Low Temp. Phys. **21**, 525 (1975).
13. J. S. Dowker and J. P. Schofield, Phys. Rev. D **38**, 3327 (1988).
14. W. G. Unruh, Phys. Rev. Lett. **46**, 1351 (1981); Phys. Rev. D **51**, 2827 (1995).
15. U. R. Fischer and M. Visser, Ann. Phys. (N.Y.) **304**, 22 (2003).
16. G. E. Volovik, JETP Lett. **65**, 491 (1997).
17. A. Junod, B. Revaz, Y. Wang, and A. Erb, Physica B (Amsterdam) **284–288**, 1043 (2000).

JETP Letters, Vol. 78, No. 12, 2003, pp. 757–758. Translated from Pis'ma v Zhurnal Éksperimental'noĭ i Teoreticheskoĭ Fiziki, Vol. 78, No. 12, 2003, pp. 1277–1278.

Increase in the Absorption Length of Inclined Extensive Air Showers

E. S. Nikiforova

Institute of Cosmophysical Research and Aeronomy, Yakut Research Center, Siberian Division, Russian Academy of Sciences, pr. Lenina 31, Yakutsk, 677891 Russia

e-mail: nikoforova@ikfia.ysn.ru

Received November 17, 2003

The dependence of the number of extensive air showers with an energy above 10^{18} eV on the zenith angle θ is obtained in groups with a constant solid-angle step. The number of showers first decreases with an increase in the zenith angle and then, after reaching ~50°, increases strongly. With increasing energy, the kink on the dependence of the number of showers on θ is displaced towards larger angles, i.e., in the direction corresponding to the shift of the depth of the cascade-curve maximum. *© 2003 MAIK "Nauka/Interperiodica".*

PACS numbers: 96.40.Pq; 96.40.De

Showers whose axes are within the perimeter of the Yakutsk EAS array are analyzed. The showers with energies above 10^{18} eV are divided into groups with a constant step in cosθ, because such a division provides the groups corresponding to a constant solid angle

$$\Omega = \int_{\theta_1}^{\theta_2} d\theta \int_0^{2\pi} d\phi \sin\theta$$

$$= 2\pi \int_{\theta_1}^{\theta_2} \sin\theta d\theta = 2\pi(\cos(\theta_1) - \cos(\theta_2)).$$

The step in cosθ is set at 0.02. The absorption length λ_ρ of charged particles at a distance of 600 m from the axis and the energy were calculated by the formulas adopted for the Yakutsk EAS array [1, 2].

Figure 1a shows the number of showers in groups as a function of zenith angle θ. Since the zenith-angle threshold for processed showers varied in different years, the number of showers with θ > 73° is somewhat underrated. The trigger threshold of charged-particle detectors can be responsible for a decrease in the number of showers with an increase in the zenith angle. Indeed, as can be seen from Fig. 1a, the number of showers decreases insignificantly in the range from 0° to ~50° and increases strongly in the range from ~50° to ~60°. The excess of inclined showers is associated with their weak absorption, i.e., with the large absorption length. With increasing zenith angle, the prevailing component of a shower changes from the electron–photon component with a short absorption length to the muon component with weak absorption.

In addition, Fig. 1 shows the zenith-angle dependence of the number of showers for other energies. The position of the kink is the same for two dependences in Fig. 1a, and the difference between these dependences has no noticeable kink in the energy range $17.8 < \log E_0 < 18.0$ (E_0 in electron volts). It can be seen that the kink in the zenith-angle dependence shifts towards larger angles with an increase in energy above 10^{18}.

To elucidate the above result, Fig. 2 shows schematically the atmospheric-depth distributions of the density ρ_{600} of charged particles for various energies. The upper curve corresponds to a higher energy. For better visualization, the absorption length changes strongly at the boundary between two regions. With increasing energy, the point at which the absorption length changes is displaced towards larger atmospheric depths in accordance with Fig. 1. The shift of the boundary can

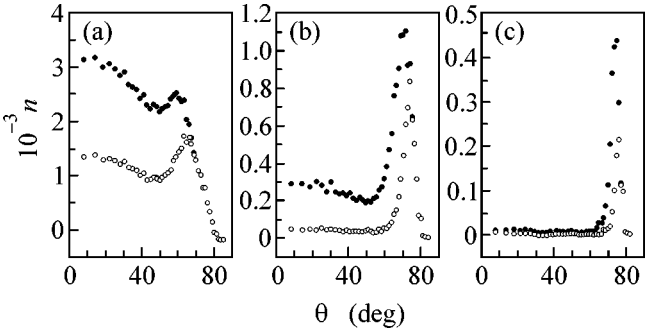

Fig. 1. Number n of showers in groups vs. the zenith angle θ for (a) $\log E_0 > 17.8$ (dark circles) and >18.0 (light circles); (b) $\log E_0 > 18.4$ (dark circles) and >18.8 (light circles); and (c) $\log E_0 > 19.2$ (dark circles) and >19.6 (light circles) (E_0 in electron volts).

0021-3640/03/7812-0757$24.00 © 2003 MAIK "Nauka/Interperiodica"

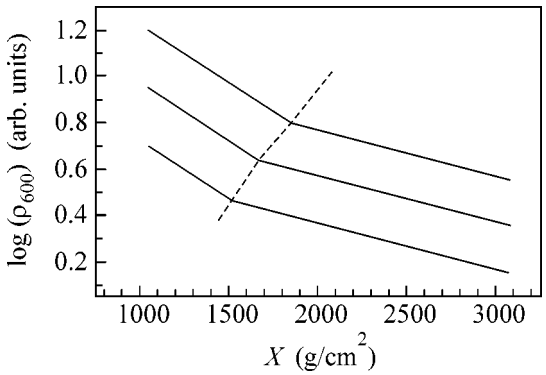

Fig. 2. Schematic atmospheric-depth distributions of the density ρ_{600} of charged particles at a distance of 600 m from the axis for various energies.

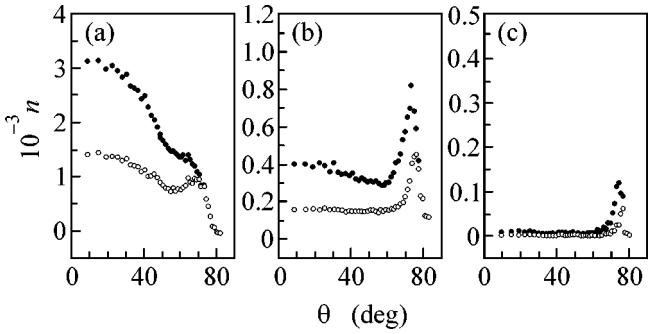

Fig. 3. The same as in Fig. 1 but for the recalculated numbers of showers.

be attributed to an increase in the depth of the cascade-curve maximum for charged particles upon an increase in energy.

The dashed line is drawn through the kink points. The energy of showers below the dashed line in Fig. 2 was recalculated with an absorption length of 800 g/cm^2 up to the dashed line and then by using the accepted formulas. Figure 3, which is similar to Fig. 1, shows the dependences obtained for recalculated showers. It can be seen that the kink shifts towards larger angles as compared to Fig. 1; i.e., an absorption length above 800 g/cm^2 must be taken for more inclined showers.

In [3], the method of equal-intensity lines for showers above 5×10^{18} eV was used to demonstrate the existence of two zenith-angle ranges (with a boundary of $\theta \sim 50°$) with noticeably different absorption lengths λ_ρ of charged particles. Figure 1 shows more clearly the existence of these two regions and the shift of the boundary between them in the direction corresponding to the shift of the depth of the cascade-curve maximum upon a variation of energy.

This study was supported by the Ministry of Industry, Science, and Technologies of the Russian Federation.

REFERENCES

1. A. V. Glushkov, I. T. Makarov, E. S. Nikiforova, *et al.*, Yad. Fiz. **58**, 1265 (1995) [Phys. At. Nucl. **58**, 1186 (1995)].
2. A. V. Glushkov, I. T. Makarov, E. S. Nikiforova, *et al.*, Astropart. Phys. **4**, 15 (1995).
3. A. A. Ivanov, V. P. Egorova, S. P. Knurenko, *et al.*, Izv. Ross. Akad. Nauk, Ser. Fiz. **65**, 1221 (2001).

Translated by R. Tyapaev

JETP Letters, Vol. 78, No. 12, 2003, pp. 759–762. From Pis'ma v Zhurnal Éksperimental'noĭ i Teoreticheskoĭ Fiziki, Vol. 78, No. 12, 2003, pp. 1279–1282.

Description of the CERN SPS Data on the Landau–Pomeranchuk–Migdal Effect for Photon Bremsstrahlung in the Quantum Regime¶

B. G. Zakharov

Landau Institute for Theoretical Physics, Russian Academy of Sciences, Moscow, 117334 Russia

Received November 11, 2003

We analyze within the light-cone path integral approach [4] the recent CERN SPS data [19] on the Landau–Pomeranchuk–Migdal effect for photon bremsstrahlung in the quantum regime from 149, 207, and 287 GeV electrons. Calculations have been carried out treating accurately the Coulomb effects and including the inelastic processes. Comparison with experiment is performed accounting for multiphoton emission. Our results are in good agreement with the data. © *2003 MAIK "Nauka/Interperiodica".*

PACS numbers: 12.20.Ds; 13.40.Hq

1. Recently, much attention has been attracted to suppression of radiation processes in media due to multiple scattering (the Landau–Pomeranchuk–Migdal (LPM) effect [1, 2]) in both QED [3–8] and QCD [4, 9–11] (for recent reviews, see [12, 13]). In QED, new interest in the LPM effect stems from the first accurate measurements of the LPM suppression by the SLAC E-146 collaboration [14] for photon bremsstrahlung from 8 and 25 GeV electrons. A detailed analysis of these high statistics data requires more accurate calculations than that performed by Migdal [2] within the Fokker–Planck approximation. The interest in the LPM effect in QCD is connected with the study of parton energy loss in a hot QCD matter, which can be produced in high-energy *AA*-collisions at RHIC and LHC.

In [4] (see also [6, 15, 16]), we developed a new approach to the LPM effect, which we call the light-cone path integral (LCPI) approach. This formalism is applicable for radiation processes in both QED and QCD. It is based on the path integral treatment of multiple scattering in the transverse coordinate representation developed in [17]. In [18], we analyzed within the LCPI approach the SLAC data [14] and obtained excellent agreement with the data. For the data of [14], the photon fractional momentum is small $x \lesssim 0.06$ ($x = k/E$, k is the photon momentum, E is the beam energy), and the LPM suppression becomes visible for $x \lesssim 0.02$, where quantum recoil effects are unimportant. In the present paper, we analyze within our approach new data on the LPM effect obtained in the CERN SPS experiment [19] for bremsstrahlung from 147, 207, and 287 GeV electrons. It is of clear interest because the SPS data allow one, for the first time, to compare theory with experiment in the kinematic region where quantum effects come into play. The kinematic range covered by the SPS data [19] is $0.01 \lesssim x < 1$, and the onset of the LPM effect occurs for $x \sim 0.1$, where quantum effects are important.

2. In the LCPI approach, the cross section of an induced $a \longrightarrow bc$ transition is expressed through the solution of a two-dimensional Schrödinger equation with an imaginary potential which is proportional to the cross section of interaction of $\bar{a}bc$ system with a medium constituent. For $e \longrightarrow \gamma e$ transition, the corresponding cross section is the dipole cross section for scattering of an e^+e^- pair off an atom, $\sigma(\rho)$ (here, ρ is the transverse distance between electron and positron), and the Hamiltonian reads

$$H = -\frac{1}{2\mu(x)}\frac{\partial^2}{\partial\boldsymbol{\rho}^2} + v(\boldsymbol{\rho}, z), \tag{1}$$

$$v(\boldsymbol{\rho}, z) = -i\frac{n(z)\sigma(|\boldsymbol{\rho}|x)}{2}, \tag{2}$$

where the Schrödinger mass is $\mu(x) = Ex(1-x)$ and $n(z)$ is the number density of the target. The longitudinal coordinate z in (1), (2) plays the role of time. The probability distribution of one-photon emission, dP/dx, is given by [4]

$$\frac{dP}{dx} = 2\mathrm{Re}\int_{-\infty}^{\infty} dz_1 \int_{z_1}^{\infty} dz_2 \exp\left(-\frac{i\Delta z}{L_f}\right) \times \hat{g}[\mathcal{H}(\boldsymbol{\rho}_2, z_2|\boldsymbol{\rho}_1, z_1) - \mathcal{H}_v(\boldsymbol{\rho}_2, z_2|\boldsymbol{\rho}_1, z_1)]\big|_{\boldsymbol{\rho}_1 = \boldsymbol{\rho}_2 = 0}. \tag{3}$$

Here, $\Delta z = z_2 - z_1$, $\mathcal{H}$ is the Green's function for the Hamiltonian (1), $\mathcal{H}_v$ is the vacuum Green's function for $v(\boldsymbol{\rho}, z) = 0$, $L_f = 2E(1-x)/m_e^2 x$, and $\hat{g}$ is the vertex

¶ This article was submitted by the author in English.

operator accumulating spin effects (for its explicit form, see [4]).

The dipole cross section can be written as $\sigma(\rho) = C(\rho)\rho^2$, where

$$C(\rho) = Z^2 C_{el}(\rho) + ZC_{in}(\rho). \quad (4)$$

Here, the terms $\propto Z^2$ and $\propto Z$ correspond to elastic and inelastic interactions of an e^+e^- pair with an atom. In the region $\rho \lesssim 1/m_e$, which is important for evaluation of the radiation rate (see below), $C_{el}(\rho)$ can be parametrized as

$$C_{el}(\rho) = 4\pi\alpha^2\left[\log\left(\frac{2a_{el}}{\rho}\right) + \frac{(1-2\gamma)}{2} - f(Z\alpha)\right],$$
$$f(y) = y^2\sum_{n=1}^{\infty}\frac{1}{n(n^2+y^2)}, \quad (5)$$

where $\alpha = 1/137$ and $\gamma = 0.577$ is Euler's constant. The $C_{in}(\rho)$ can be written in a similar form (with a_{el} replaced by a_{in}) but without $f(Z\alpha)$. The parametrization of $C_{el}(\rho)$ corresponds to scattering of and e^+e^- pair on the atomic potential $\phi(r) = (Ze/4\pi r)\exp(-r/a_{el})$. The first two terms in the square brackets on the right-hand side of (5) stem from the Born approximation, while the last one gives the Coulomb correction due to multiphoton exchanges. To account for the finite size of nucleus, one should replace on the right-hand side of (5) ρ by R_A for $\rho \lesssim R_A$ (here, R_A is the nucleus radius).

The parameters a_{el} and a_{in} can be adjusted by comparing the Bethe–Heitler cross section calculated via the dipole cross section [6]

$$\frac{d\sigma^{BH}}{dx} = \int d\boldsymbol{\rho}\left|\Psi_e^{e\gamma}(x, \boldsymbol{\rho})\right|^2\sigma(\rho x) \quad (6)$$

(here, $\Psi_e^{e\gamma}(x, \boldsymbol{\rho})$ is the light-cone wave function for the $e \longrightarrow e\gamma$ transition) with that obtained within the standard approach using the Thomas–Fermi–Molier model [20]. This gives $a_{el} = 0.81r_BZ^{-1/3}$ and $a_{in} = 5.3r_BZ^{-2/3}$ [18].

Treating the potential (2) as a perturbation, one can represent the spectrum (3) as

$$\frac{dP}{dx} = \frac{dP^{BH}}{dx} + \frac{dP^{abs}}{dx}, \quad (7)$$

where the first term

$$\frac{dP^{BH}}{dx} = nL\frac{d\sigma^{BH}}{dx} \quad (8)$$

is the Bethe–Heitler spectrum (L is the target thickness) and the second one is the absorptive correction responsible for LPM suppression [6]. We use this representation for the numerical calculations. The explicit form of the absorptive term and light-cone wave function entering (6) can be found in [6].

An important characteristic of the LPM effect is the in-medium coherence (formation) length of photon emission (we refer to it as L_f^{eff}). In the sense of representation (3), L_f^{eff} is simply the typical Δz. The L_f^{eff} is related to the dominating ρ scale, ρ_{eff}, via the diffusion relation $\rho_{\text{eff}} \sim \sqrt{2L_f^{\text{eff}}/\mu(x)}$. From it follows that, for small LPM suppression (when $L_f^{\text{eff}} \sim L_f$), $x\rho_{\text{eff}} \sim 1/m_e$. For strong LPM effect, L_f^{eff} and ρ_{eff} are determined by the interplay of the diffusion and absorption effects. From the diffusion relation and condition $nL_f^{\text{eff}}\sigma(x\rho_{\text{eff}})/2 \sim 1$, saying that absorption for the $e^+e^-\gamma$ system becomes strong at $\Delta z \sim L_f^{\text{eff}}$, one obtains $x\rho_{\text{eff}} \sim 1/m_e\sqrt{\eta}$, and $L_f^{\text{eff}} \sim L_f/\eta$, where $\eta = 2[nE(1-x)C(1/m_e)/xm_e^4]^{1/2}$. Thus, one sees that, as was said above, the spectrum is only sensitive to the behavior of $C(\rho)$ at $\rho \lesssim 1/m_e$.

Note that the Fokker–Planck approximation in momentum representation used in Migdal's analysis [2] corresponds to the replacement of $C(\rho)$ by $C(\rho_{\text{eff}})$. Then, the spectrum can be written via the oscillator Green's function. This approximation works well for strong LPM effect ($\eta \gg 1$), when the logarithm in (5) is much larger than unity. For the SPS conditions, $\eta \lesssim 3$ and the logarithm in (5) is ~4–5. In such a regime, neglecting the logarithmic dependence of $C(\rho)$ may give errors of about 10–20%.

3. In [19], the experimenters used Ir target with thickness $L = 4.36\%\ X_0 = 0.128$ mm, where X_0 is the radiation length, for Ir $X_0 \approx 2.94$ mm [20]. The spectra in the radiated energy were measured for $k > 2$ GeV. Similarly to the SLAC data, the SPS spectra include multiphoton emission. Using the estimate given above for L_f^{eff}, one can see that, for the SPS conditions, L_f^{eff}/L does not exceed ~0.02–0.04. The smallness of this quantity allows one to evaluate multiphoton emission in the probabilistic approach.

We write the spectrum in the radiated energy (we refer to it as dN/dx) as

$$\frac{dN(E, x)}{dx} = K(E, x)\frac{dP(E, x)}{dx}, \quad (9)$$

where $K(E, x)$ accounts for multiphoton effects. For the SPS kinematic domain, N-photon emission with $N > 2$ can be neglected. Then, in the probabilistic treatment of the radiation of one and two photons, one can obtain for $K(E, x)$[1]

[1] This is a generalization to arbitrary x of the low-x K factor derived in [18].

$$K(E,x) = \exp\left[-\int_x^1 dy \frac{dP(E,y)}{dy}\right]\left[1+\frac{1}{2}F(E,x,\delta)\right], \quad (10)$$

$$F(E,x,\delta) = \int_\delta^{\delta/(1-x)} dy \frac{dP(E,y)}{dy} + \int_\delta^1 dy\left[\frac{dP(E,y)}{dy} - \frac{dP(E(1-x),y)}{dy}\right] - \int_\delta^{x-\delta} dx_1\left[\frac{dP(E,x_1)}{dx_1} + \frac{dP(E,x_2)}{dx_2} - \frac{1}{1-x_1} \times \frac{dP(E,x_1)}{dx_1}\frac{dP(E(1-x_1),y_2)}{dy_2}\left(\frac{dP(E,x)}{dx}\right)^{-1}\right], \quad (11)$$

where $x_2 = x - x_1$, $y_2 = x_2/(1-x_1)$, $\delta = k_{\min}/E$. Although the expression (11) is infrared finite, we indicated explicitly dependence on the low-energy cutoff $k_{\min}$. In our numerical calculations, we take $k_{\min} = 0.1$ GeV. The results are practically insensitive to variation of this quantity. The inaccuracy of the above expression for the K factor at the SPS conditions is $\lesssim 0.5\%$. This is clearly no worse than the accuracy of the probabilistic approach by itself.

4. In the figure, we plotted the SPS data and our results obtained with (solid line) and without (dashed line) LPM suppression. In [19], the spectra in the radiated energy were presented in logarithmic bins (25 per decade). It corresponds to $rdN/d\log(k)$ with $r = 2\tanh(\Delta/2)$, $\Delta = \log(10)/25$. This form is used in the figure. Besides the multiphoton emission, we have taken into account photon absorption, multiplying the theoretical spectra by $\langle K_{abs}\rangle \approx 1 - L/2\lambda_{ph}$, where λ_{ph} is the photon attenuation length. This decreases the spectra by $\lesssim 1.5\%$. The theoretical spectra were multiplied by normalization coefficients, C_{norm}, that were adjusted at each energy to minimize χ^2. We obtained the values $C_{\text{norm}} = 0.994 \pm 0.006$ ($\chi^2/N = 1.08$), 0.982 ± 0.005 ($\chi^2/N = 1.78$), and 0.944 ± 0.004 ($\chi^2/N = 1.43$) for $E =$ 287, 207, and 149 GeV, respectively. One can see that the theoretical spectra (with LPM suppression) are in good agreement with the data.

5. To summarize, we have analyzed the recent SPS data [19] on the LPM effect for bremsstrahlung from 149, 207, and 287 GeV electrons. The calculations have been performed within the light-cone path integral formalism [4, 6]. We treat accurately the Coulomb effects and include the inelastic processes. The comparison with experiment is performed accounting for multiphoton emission and photon absorption. Our results are in good agreement with the data in the full studied kinematic range, which includes the region of the onset of the LPM effect where the photon fractional momentum $x \sim 0.1$ and quantum recoil effects are important.

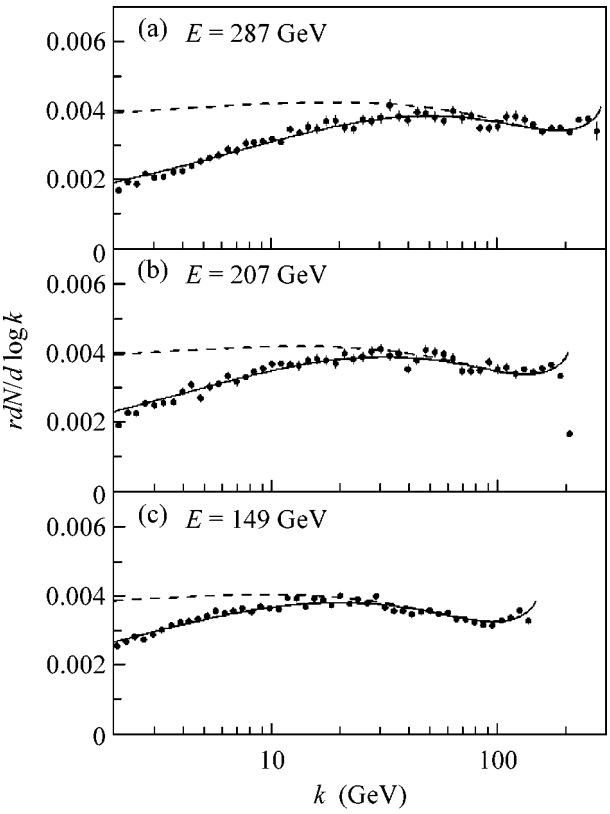

Comparison of the spectra in the radiated energy from the SPS experiment [19] with our calculations for bremsstrahlung from (a) 287, (b) 207, and (c) 149 GeV electrons on $4.36\%X_0$ Ir target. The solid line shows our results with LPM suppression. The dashed line shows the Bethe–Heitler spectrum. The multiphoton emission and photon absorption are taken into account. The Bethe–Heitler spectra are multiplied by the normalization coefficients obtained for the spectra with LPM suppression.

I am grateful to U.-G. Meiβner and J. Speth for the hospitality at FZJ, Jülich, where this work was completed. I would also like to thank U.I. Uggerhøj for sending the files of the experimental data and comments about some aspects of the SPS experiment. This work was supported in part by DFG, grant no. 436RUS17/72/03.

REFERENCES

1. L. D. Landau and I. Ya. Pomeranchuk, Dokl. Akad. Nauk SSSR **92**, 535 (1953); Dokl. Akad. Nauk SSSR **92**, 735 (1953).
2. A. B. Migdal, Phys. Rev. **103**, 1811 (1956).
3. R. Blankenbecler and S. D. Drell, Phys. Rev. D **53**, 6265 (1996).
4. B. G. Zakharov, Pis'ma Zh. Éksp. Teor. Fiz. **63**, 906 (1996) [JETP Lett. **63**, 952 (1996)].

5. R. Baier, Yu. L. Dokshitzer, A. H. Mueller, *et al.*, Nucl. Phys. B **478**, 577 (1996).
6. B. G. Zakharov, Pis'ma Zh. Éksp. Teor. Fiz. **64**, 737 (1996) [JETP Lett. **64**, 781 (1996)].
7. R. Blankenbecler, Phys. Rev. D **55**, 190 (1997).
8. V. N. Baier and V. M. Katkov, Phys. Rev. D **57**, 3146 (1998).
9. R. Baier, Yu. L. Dokshitzer, S. Peigne, and D. Schiff, Phys. Lett. B **345**, 277 (1995).
10. R. Baier, Yu. L. Dokshitzer, A. H. Mueller, *et al.*, Nucl. Phys. B **483**, 297 (1997).
11. B. G. Zakharov, Pis'ma Zh. Éksp. Teor. Fiz. **65**, 585 (1997) [JETP Lett. **65**, 615 (1997)].
12. S. R. Klein, Rev. Mod. Phys. **71**, 1501 (1999).
13. R. Baier, D. Schiff, and B. G. Zakharov, Annu. Rev. Nucl. Part. Sci. **50**, 37 (2000).
14. P. L. Anthony, R. Becker-Szendy, P. E. Bosted, *et al.*, Phys. Rev. D **56**, 1373 (1997).
15. B. G. Zakharov, Phys. At. Nucl. **61**, 838 (1998).
16. B. G. Zakharov, JETP Lett. **70**, 176 (1999).
17. B. G. Zakharov, Sov. J. Nucl. Phys. **46**, 92 (1987).
18. B. G. Zakharov, Phys. At. Nucl. **62**, 1008 (1999).
19. H. D. Hansen, U. I. Uggerhøj, C. Biino, *et al.*, Phys. Rev. Lett. **91**, 014801 (2003).
20. Y.-S. Tsai, Rev. Mod. Phys. **46**, 815 (1974).

JETP Letters, Vol. 78, No. 12, 2003, pp. 763–767. Translated from Pis'ma v Zhurnal Éksperimental'noĭ i Teoreticheskoĭ Fiziki, Vol. 78, No. 12, 2003, pp. 1283–1288.

Physics of Collective Attraction of Negatively Charged Dust Particles

V. N. Tsytovich

Institute of General Physics, Russian Academy of Sciences, ul. Vavilova 38, Moscow, 119991 Russia

e-mail: tsytov@lpi.ru

Received October 17, 2003; in final form, November 13, 2003

A physical interpretation is proposed for the collective attraction of dust particles, leading to pairing of likely (negatively) charged dust particles, the formation of dust molecules, and the emergence of other complexes containing a large number of dust particles (in the limit, dust plasma crystals). The value of the spacing between particles in such dust structures estimated on the basis of the proposed mechanism of attraction corresponds to the observed interparticle distances in the crystal lattices of recently discovered plasma-dust crystals. The proposed mechanism may form the basis for interpreting various phenomena frequently observed in dusty plasmas. © *2003 MAIK "Nauka/Interperiodica".*

PACS numbers: 52.27.Lw

1. The ease of obtaining the first dust crystals [1–4] by injecting dust particles into a low-temperature plasma, as well as numerous indirect experimental indications of the fact that rather strong attractive forces may act between likely charged dust particles starting from a certain spacing between them [5–7], stimulated an intense search for a possible mechanism of attraction [8–14]. Some of the observed phenomena, such as (i) the Leseage effect or shadow attraction [8–10], when a dust particles screens plasma flows to another dust particle, and (ii) the effect of accumulation of positive charges in the wake of an ion flow [11, 12], which is precisely the Vavilov–Cherenkov effect of emission of dust or plasma waves in a reference frame moving with the ion flow, have indisputable physical foundations. Analysis shows that such effects operate for individual particles but not for large complexes of particles. For example, the strong attraction in the wake operates only for downflow particles in an ion flow and can be used for interpreting the interaction of a few particles (two isolated particles as well as particles in several dust layers or in planar dust two-layer crystals). These effects require a rather strong external electric field for creating a supersonic ion flow; such fields indeed exist in the wall boundary layer, where dust crystals were discovered. It is now clear, however, that this mechanism cannot dominate in most experiments. Even the first experiment proved the existence of crystals with up to 15 layers separated from one another by distances on the order of the distance over which the potential drop takes place at the wall. The first layer might be in a supersonic flow (Bohm's criterion for the wall boundary layer is that the ratio of the flow velocity to the sound velocity, i.e., the Mach number, must be greater than unity at the wall layer boundary and not much larger than $M \approx 2$–3 at the wall). The next layers are in much weaker fields (in the so-called pre-sheath) and, hence, in much smaller ion fluxes, for which the Mach number $M < 1$ and the mechanism of attraction in the wake of the flow does not operate. In subsequent experiments [15, 16], dust crystals were observed in the strata of a glow discharge, where the electrostatic potential drop is much smaller than in the wall boundary layer (approximately by a factor of 3–5). The observation of dust crystals with approximately the same distances between particles rules out the wake mechanism of attraction for all layers. Finally, the results of recent experiments on observation of dust crystals containing more than 1000 layers in the bulk plasma obviously contradict the wake mechanism. The wake attraction mechanism, as well as the Leseage mechanism of shadow attraction, operates only for a small number of particles; in this limit, these two mechanism might compete (the corresponding estimates are given below together with estimates of the attraction mechanism considered here). The third possible collective mechanism of attraction was discussed in [13, 14] for a large system containing a large number of dust particles, so that plasma flows from different particles become inseparable (in contrast to the Leseage attraction, when the flows to individual particles can be separated). Since such flows are collective, the attraction is also referred to as collective. Collective attraction was obtained via the proof that the static permittivity changes its sign for small values of wave number (at large distances). However, this phenomenon was not analyzed comprehensively from the standpoint of physics and its analysis involved a number of computational difficulties. In addition, the passage of the static permittivity through zero for real values of wave numbers

(which means that repulsion changes for attraction) leads to the problem of bypassing of poles in the calculation of the potential of particles. In the case under investigation, the latter problem is as fundamental as the problem of bypassing of poles in Landau damping for plasma modes [17]. In [14], we evaluated integrals via half-residues at the poles on the real axis, which requires both exact substantiation and the determination of applicability limits. Such a problem cannot be solved without a deeper analysis of physical processes leading to the collective attraction effect. This communication is devoted to the physics of processes leading to collective attraction and aims at the proof that the problem can be solved consistently only by taking into account the finite size of dust particles in the response of a dusty plasma to a dust charge introduced into it as well as in the boundary conditions at the surfaces of dust particles introduced into the plasma. In [14], we derived the permittivity, taking into account the finite size of particles, but the field was calculated as the field produced by point particles, assuming that their size is much smaller than the Debye screening radius. Here, we will derive specific inequalities for the cases when the results for finite-size dust particles coincide with those obtained in [14] for nearly pointlike particles; the bypassing rules used in [14] will be confirmed in this limit. The problem generalizing the result obtained in [14] will be solved for particles of an arbitrary size.

We will derive more general relations, from which the results of [14] can be obtained as a limiting case. All calculations will be made for inequalities closest to the experimental results. The estimated distance between particles corresponds to the observed value to a satisfactory degree of accuracy. This leads to the conclusion that the mechanism considered here could be treated as the main mechanism for the observed formation of plasma crystals, which makes it possible to describe main processes in a system with a large number of dust particles in other states of aggregation of dust systems (gaseous or liquid), preceding crystallization. The reviews of the state of the art for the given problem can be found in [18–22].

2. Systems with a large number of dust particles can exist in a steady state without sustaining the plasma adsorption at dust particles by external ionization sources because the mean free path of plasma particles before they are adsorbed at dust particles in contemporary experiments is one to three orders of magnitude smaller than the size of the systems (setups) in which the condensation of a dusty plasma into plasma crystals was observed. Spatial recombination or destruction of plasma particles at the walls of the experimental setup does not play any significant role in the experiments. Such systems are essentially nonequilibrium (athermal) and the sign reversal of the static permittivity does not contradict the general principles, which are valid only for systems in thermal equilibrium. The Leseage and wake mechanisms operate only in the opposite limit, when the size of the system is much smaller than the mean free path for plasma particles before they are adsorbed at dust particles. In the presence of adsorption on dust, the ground state of the system must be determined not only by the quasineutrality condition but also by the balance between ionization and adsorption. It is convenient to use the normalization conditions generally accepted for studying dusty plasmas: the number densities n and n_e of ions and electrons and the charge density $Z_d n_d$ of the dust should be normalized to the steady-state value of ion number density n_0 by introducing the Havnes parameter $P = n_d Z_d / n_0$. Distances r and sizes a of dust particles are normalized to the ionic Debye radius, bearing in mind that $\tau = T_i / T_e \ll 1$ in most experiments and the ionic Debye radius is close to the total Debye radius. The ion drift velocity u is normalized to $v_{Ti}/\sqrt{2}$, where $v_{Ti} = \sqrt{T_i/m_i}$ is the mean thermal velocity of ions.

In this case, the ground state of the plasma is determined by only one parameter P_0; from the quasineutrality condition for this state, we obtain $n_{e,0} = 1 - P_0$. The dimensionless charge of particles, $z = Z_e e^2 / a T_e$, in the ground state is denoted by z_0 and is determined from the condition of charging. It depends only on P_0, τ, and the ratio of the masses of electrons and ions. For a fixed gas and for a fixed value of τ, this charge is determined by P_0 alone; in the ground state, z_0 is usually on the order of unity. Assuming that ionization is uniform and proportional to the electron density, we can also express the ionization coefficient in terms of P_0 by using the fact that the second condition (the balance of adsorption and ionization) holds in the ground state. Then, the continuity equation for the ion flow can be written in the form

$$\frac{1}{r^2}\frac{d}{dr} r^2 n u = a \alpha_{\rm ch} P_0 \left(\frac{n_e}{1 - P_0} - \frac{nP}{P_0} \right),$$
$$\frac{1}{r^2}\frac{d}{dr} r^2 \frac{d}{dr}\frac{\psi}{r} = \frac{1}{r}\frac{d^2 \psi}{dr^2}, \qquad (1)$$

where $\alpha_{\rm ch}$ is the coefficient of capture (adsorption) of plasma ions by dust particles; in simple models, this coefficient is equal to $1/2\sqrt{\pi}$. Balance equation (1) holds in the ground state $n = 1$, $n_{e/0} = 1 - P_0$, $P = P_0$. A dusty plasma basically differs from an ordinary plasma in that these relations must be satisfied for it in the ground state.

3. A physical interpretation for the mechanism of formation of attractive regions is that the perturbation of the ground state by another particle or charge introduced into the plasma leads to the formation of space charge regions in the polarization charge surrounding the introduced charge. The sign of the space charge is opposite to that of the charge screening the field of the introduced charge. The essence of the effect is the formation of ion flows carrying ions from the regions in which the ionization exceeds adsorption (due to the

perturbation of the ground state by the external charge) to the regions where adsorption exceeds ionization. Plasma flows result in the formation of regions where a positive charge is accumulated, which alternate with the regions of accumulation of a negative charge. The accumulation of positive charges must be stabilized by the accumulated charge itself, reflecting excess charges. The effects become weaker with increasing distance from the introduced charge. The presence of such steady-state flows generated by the introduced charge is a new effect leading to attraction and pairing of dust particles (to a certain extent, this is equivalent to Cooper pairing) and the dusty plasma becomes a system consisting of dust molecules. A decrease in temperature leads to the formation of complexes of dust particles and, in the long run, dust crystals. Such processes do not take place in ordinary plasmas; any charge introduced into the plasma is screened so that only polarization charges of the same polarity are formed around this charge (a positive charge is screened by an excess of electrons and deficit of ion; accordingly, a negative charge is screened by a deficit of electrons and an excess of ions).

The present analysis differs significantly from previous studies in a consistent treatment of an external charged dust particle of size a and the determination of required boundary conditions on the particle surface from physical considerations.

Let us consider a region outside of the added charge and introduce a factor ψ via the relation $e\phi = -Z_d e^2\psi/r$ (Z_d is the charge of the introduced dust particle in units of electron charge). The ion density perturbation can be written in the form $\delta n = N/r$. In view of the adiabaticity of the electron distribution, we have $\delta n_e/n_{e,0} = \delta n_e/(1 - P_0) = -z_0 a\psi/r$. We denote by G the difference $\psi - \tau N/z_0 a$. The balance equation for the forces acting on ions (forces of the electrostatic field, forces of ionic pressure, and drag forces induced by the dust in the ground state) leading to the appearance of ion flows around the introduced charge assumes the simple form

$$\frac{d}{dr}\left(\frac{G}{r}\right) = \alpha_{dr} P_0 n u. \tag{2}$$

Here, the coefficient of ion drag by the dust in the simplest model [18–23] is equal to $\alpha_{dr} = 2\ln\Lambda/3\sqrt{\pi}$ (the effective Coulomb logarithm $\ln\Lambda$ may include collective phenomena in dusty plasmas). Perturbations arise not only in the number densities of electrons and ions (which induce ion flows) but also in the variations of the charge of the background dusty plasma, $\delta P/P_0 = \delta z/z_0 = 1/(z_0 + 1)(\delta n_e/n_{e,0} - \delta n)$. Although the latter effect should be taken into account, it does not introduce any qualitative changes and only leads to the emergence of numerical factors $z_0/(1 + z_0)$ on the order of unity in the coefficients describing the effects of attraction. It is remarkable that (in the case of spherical symmetry) the combination of Eqs. (1) and (2) together with the Poisson equation leads to the following two linear equations containing second-order derivatives with respect to the distance from the center of the introduced charge:

$$\frac{d^2G(r)}{dr^2} = k_0^2(G - (1 + \tau)\psi); \qquad k_0^2 = \frac{\alpha_{dr}\alpha_{ch} z_0^2 a^2 P_0^2}{(1 + z_0)\tau}, \tag{3}$$

$$\frac{d^2\psi(r)}{dr^2} = \left(1 + \frac{P_0}{1 + z_0} + \tau\left(1 - \frac{P_0 z_0}{1 + z_0}\right)\right) - \left(1 + \frac{P_0}{1 + z_0}\right)G(r). \tag{4}$$

Taking into account that the coefficients in Eqs. (3) and (4) a real and discarding the solutions increasing indefinitely with increasing distance r, we can write the solution of this system in the form

$$\psi(r) = \psi_E \exp(-k_E r) + \psi_C \cos(k_C r), \tag{5}$$

$$k_E = \sqrt{\frac{R + S}{2}}; \quad k_C = \sqrt{\frac{R - S}{2}}; \qquad R = \sqrt{S^2 + 4k_0^2 P_0 \tau}, \tag{6}$$

$$S = k_0^2 + 1 + \frac{P_0}{1 + z_0} + \tau\left(1 - \frac{P_0 z_0}{1 + z_0}\right). \tag{7}$$

The second alternating term in Eq. (5) describes a system of attractive potential wells, decreasing with increasing distance (in order to obtain the potential energy of another dust particle of charge Z_d, Eq. (5) should be multiplied by $Z_d z a T_e/r$). Thus, effects of attraction arise for any boundary conditions leading to a nonzero value of ψ_C. This effect has nothing in common with the sign variation of the interaction in the presence of external ion flows [11]. In the effect considered here, the perturbations produced by the introduced charge induce plasma flows rather than currents and create additional concentration and rarefaction of the polarization charge, leading to the formation of the regions of attraction for charges. Below, we will consider comparative estimates of various effects of attraction and demonstrate that collective attraction is the strongest even in the presence of an additional external ion flow.

4. The first natural requirement is that the total central charge must be equal and opposite to the total external polarization charge. Analysis shows that this requirement can be reduced to the form

$$\psi(a) - a\left.\frac{d\psi(r)}{dr}\right|_{r = a} = 1. \tag{8}$$

Another requirement is that the change in the power in the outer region must be equal to the power adsorbed by the entire surface of the introduced charge:

$$a\frac{dG(r)}{dr}\bigg|_{r=a} - G(a) = w;$$
$$w = \alpha_{dr}P_0 a(4\pi a^2 nu|_{r=a}). \tag{9}$$

This flux changes the charge of the introduced dust particle. In the framework of the approach described here, this change is small so that we can set, for example, $w = 0$ (however, the case of an adsorbing particle can also be considered). In this limit, we obtain

$$\psi_E = \frac{\exp(k_E a)}{(1+k_E a)}\left[\frac{k_E^2 - k_0^2}{k_E^2 + k_C^2}\right]; \tag{10}$$

$$\psi_C = \frac{1}{\cos(k_C)a + k_C a\sin(k_C a)}\left[\frac{k_C^2 + k_0^2}{k_E^2 + k_C^2}\right]. \tag{11}$$

These expressions make it possible to estimate the limits of applicability for the pole bypassing rules and the assumption concerning the pointlike nature of the charge, which were used in [14]. For the term containing cosine and leading to collective attraction, the most severe constraint appears in the limit $k_0 \ll 1$ and boils down to $a^2 \ll 1$; in other words, the particle size must be much smaller than the ionic Debye radius. This constraint is expected from the standpoint of physics and the value of attraction coincides with that determined in [14]. For $k_0 \gg 1$ (when the collective attraction effects are the strongest), the range of applicability of the results obtained in [14] for collective attraction expands considerably, $a \ll 1/\sqrt{P_0\tau}$ (the right-hand side of the inequality is considerably greater than unity for the existing experimental conditions). For the term with exponential screening, we find that the result obtained in [14] is valid for $a \ll 1$ when $k_0 \ll 1$, while for $k_0 \gg 1$, this result is valid only for $a^2 \ll \sqrt{\tau}$ (this condition is often satisfied for the existing experimental parameters). We can write the solutions for $a \ll 1$ in the limiting cases:

$$\psi = \exp\left(-\sqrt{\left(1 + \frac{P_0}{1+z_0} + \tau\left(1 - \frac{z_0 P_0}{1+z_0}\right)\right)}(r-a)\right)$$
$$+ \frac{k_0^2}{1 + \frac{P_0}{1+z_0} + \tau\left(1 - \frac{z_0 P_0}{1+z_0}\right)} \tag{12}$$
$$\times \cos\left(\frac{k_0 r\sqrt{P_0\tau}}{\sqrt{1 + \frac{P_0}{1+z_0} + \tau\left(1 - \frac{z_0 P_0}{1+z_0}\right)}}\right)$$

for $k_0 \ll 1$ and

$$\psi = \frac{P_0}{(1+z_0)k_0^2(1+k_0 a)}\exp(-k_0(r-a)) + \cos(\sqrt{P_0\tau}r) \tag{13}$$

for $k_0 \gg 1$.

For $k_0 \gg 1$, the exponential part is strongly suppressed by factor $1/k_0^2$ for $k_0 a \gg 1$ as well (i.e., when the inequality $a^2 \ll \sqrt{\tau}$ holds); in this case, the results obtained in [14] are inapplicable, the exponential part is suppressed even more strongly (in accordance with the results obtained in this study), and attraction dominates in a wider range of particle sizes.

5. The fulfillment of conditions (8) and (9) is verified for solutions (5)–(7), (10), and (11) by using the condition of adiabaticity breaking at infinity (in the integration of the term containing cosine), which means taking into account the adsorption (e.g., on neutrals) followed by the consideration of the limit when such adsorption tends to zero. Thus, this situation is not trivial from the standpoint of physics. The above statement concerning the method of regularization was verified by calculations taking into account the drag due to neutrals.

For most typical experimental parameters, $k_0 \approx 3$ and corresponds to an intermediate between limiting cases (12) and (13). In this case, the distance between particle is estimated as 250–300 μm, which is in satisfactory agreement with the observed spacing in clusters and crystals. Although the Leseage and wake attractions correspond to the limit opposite to collective attraction, these modes can be compared for hybrid systems, in which a small number of large particles are located in a system of a large number of small particles. Experiments of this type have been made for two sizes of particle [23]. The condition of predominance of the collective attraction over the Leseage attraction is satisfied easily, since the collective attraction contains additional parameter $1/\tau \approx 10^2$. Assuming that the product of $\alpha_{dr}\alpha_{ch} \approx 1/10 - 1/3$, we can state that the collective attraction dominates approximately by one and a half orders of magnitude. As regards the wake attraction, it can be on the order of the Leseage attraction if $a^3 \approx \sqrt{\tau}/M$ (M is the Mach number), while the condition of predominance of the collective attraction over the wake attraction assumes the form

$$a^2 \gg \frac{\tau}{M} \tag{14}$$

and holds in most existing experiments, in which the left-hand side of inequality (14) is on the order of 1/10 and the right-hand side is on the order of 1/100 (estimates are made under the assumption that the sizes of different particles are of the same order of magnitude).

Thus, the treatment of poles in the collective attraction is substantiated in this case and is connected not with instability but with correct interpretation of finiteness of the particle size. Naturally, instability exists and leads to transformation of the system either to a system of paired dust particles or to a system of other complexes (including plasma crystals). Instabilities develop at a comparatively slow rate; consequently, the analysis of interaction and attraction of dust particles prior to the full development of instability (as was done above) is well grounded (especially for bulk particles). Such a treatment makes it possible to describe a nonlinear collective attraction by taking into account the Gurevich–Parker effects [24, 25]. A description of collective attraction in the presence of ion flows (collective attraction in the wake), which was studied in [20, 26], also should not involve considerable difficulties.

This study was supported by INTAS and the Russian Foundation for Basic Research (grant no. 0202-16439).

REFERENCES

1. H. Thomas, G. Morfill, V. Demmel, and J. Goree, Phys. Rev. Lett. **73**, 652 (1994).
2. J. H. Chu and I. Lin, Physica A (Amsterdam) **205**, 183 (1994).
3. A. Melzer, T. Trottenberg, and A. Piel, Phys. Lett. A **191**, 301 (1994).
4. Y. Hayashi and K. Tachibana, Jpn. J. Appl. Phys., Part 1 **33**, L804 (1994).
5. E. B. Tomme, B. M. Annaratone, and J. E. Allen, Plasma Sources Sci. Technol. **9**, 87 (2000).
6. J. E. Allen and B. M. Annoratone, J. Plasma Phys. **7**, 397 (1999).
7. Y. Hayashi and A. Sawai, in *Proceedings of the Second International Conference of Dusty Plasmas-ICPDP-99*, Ed. by Y. Nakamura, T. Yakota, and P. K. Shukla (Elsever, Amsterdam, 2000), p. 83.
8. V. N. Tsytovich, Y. Khodataev, and R. Bingham, Comments Plasma Phys. Control. Fusion **17**, 249 (1996).
9. A. S. Ignatov, Comments P.N. Lebedev Inst. **1**, 58 (1995).
10. Ya. K. Khodataev, G. Morfill, and V. N. Tsytovich, J. Plasma Phys. **65**, 257 (2001).
11. S. Vladimirov and M. Nambu, Phys. Rev. E **52**, R2172 (1995).
12. S. V. Vladimirov and O. Ishihara, Phys. Plasmas **2**, 444 (1996).
13. V. N. Tsytovich and U. de Angelis, Phys. Plasmas **8**, 1141 (2001).
14. V. N. Tsytovich and G. Morfill, Fiz. Plazmy (Moscow) **28**, 195 (2002) [Plasma Phys. Rep. **28**, 171 (2002)].
15. V. E. Fortov, A. P. Nefedov, O. F. Petrov, *et al.*, Phys. Lett. A **219**, 89 (1996).
16. V. E. Fortov, A. P. Nefedov, O. F. Petrov, *et al.*, Phys. Rev. E **54**, R2236 (1996).
17. L. D. Landau, Zh. Éksp. Teor. Fiz. **16**, 574 (1946); V. N. Tsytovich, *Lectures on Nonlinear Plasma Kinetics* (Springer, Berlin, 1995), p. 47.
18. V. N. Tsytovich, Usp. Fiz. Nauk **167**, 57 (1997) [Phys. Usp. **40**, 53 (1997)].
19. V. N. Tsytovich, G. Morfill, and H. Thomas, Fiz. Plazmy (Moscow) **28**, 675 (2002) [Plasma Phys. Rep. **28**, 623 (2002)].
20. G. Morfill, V. N. Tsytovich, and H. Thomas, Fiz. Plazmy (Moscow) **29**, 3 (2003) [Plasma Phys. Rep. **29**, 1 (2003)].
21. H. Thomas, G. Morfill, and V. N. Tsytovich, Fiz. Plazmy (Moscow) **29**, 963 (2003) [Plasma Phys. Rep. **29**, 895 (2003)].
22. V. Tsytovich, G. Morfill, and H. Thomas, Fiz. Plazmy (Moscow) **30** (2004) (in press).
23. A. Nefedov, G. Morfill, V. Fortov, *et al.*, New J. Phys. **5**, 33 (2003).
24. Ya. L. Al'pert, A. V. Gurevich, and L. P. Pitaevskiĭ, *Space Physics with Artificial Satellites* (Nauka, Moscow, 1964; Consultants Bureau, Washington, 1965).
25. J. Lafranbose and L. Parker, Phys. Fluids **16**, 629 (1973).
26. R. Kompaneetz and V. Tsytovich, Contrib. Plasma Phys. (2003) (in press).

Translated by N. Wadhwa

JETP Letters, Vol. 78, No. 12, 2003, pp. 768–771. Translated from Pis'ma v Zhurnal Éksperimental'noĭ i Teoreticheskoĭ Fiziki, Vol. 78, No. 12, 2003, pp. 1289–1292.

Charge Accumulation in Ge Quantum Dots in a GaAs/ZnSe/QD–Ge/ZnSe/Ge Floating Gate Transistor Structure

I. A. Litvinova, I. G. Neizvestnyĭ, A. V. Prozorov, S. P. Suprun, V. N. Sherstyakova, and V. N. Shumskiĭ

Institute of Semiconductor Physics, Siberian Division, Russian Academy of Sciences, Novosibirsk, 630090 Russia

Received November 6, 2003

A GaAs/ZnSe/QD–Ge/ZnSe/Ge germanium-quantum-dot floating-gate transistor structure is obtained and investigated by molecular beam epitaxy. It has been shown that a positive change in the channel current is observed upon light illumination with wavelengths longer than 0.5 μm and a negative change is observed for shorter wavelengths, which is associated with charging of quantum dots. Measurements of relaxation curves after switching off the illumination show that the decay of the current lasts for from tens of seconds to several hours, depending on the temperature of the sample. The changes in the channel current and relaxation curves indicated above are explained based on the existence of three types of transitions in quantum dots upon radiation absorption with allowance made for the variation of the channel state near the heteroboundary from depletion to inversion as a result of charge accumulation in quantum dots. © *2003 MAIK "Nauka/Interperiodica".*

PACS numbers: 73.21.La; 73.63.Kv; 78.67.Hc

At present, in connection with the development of nanotechnologies, works have appeared in which the possibility of creating memory elements based on single-electron field-effect transistors is discussed. In these transistors, one bit of information corresponds to an electron trapped in a quantum dot (QD) arranged between the control gate and the channel. Such a memory element operating at room temperature was described in [1]. A QD 7×7 nm in size was the floating gate of a silicon MOS transistor with a channel width of about 10 nm, which was smaller than the Debye shielding radius of an electron. In this case, one electron trapped in the QD fully screened the potential of the control gate, which led to a significant shift in the threshold voltage. Electron tunneling into the QD took place upon applying a pulse voltage across the control gate and the channel. The starting structure was created with the use of self-aligned technologies that involve electron-beam lithography, reactive ion etching, precision thermal oxidation, and plasma-enhanced chemical vapor deposition, which allowed the structure sizes indicated above to be obtained.

Along with the development of the technology of fabricating individual QDs, a field is developed associated with the fabrication of assemblies of quantum dots (AQDs) in Ge/Si and AlGaAs/GaInAs systems [2–5]. In the future, AQD systems should find use in the field of creating high-performance lasers based on III–V compounds and also other devices such as photodetectors and transistors based on Ge/Si.

Over a period of years, we have been investigating the properties of assemblies of QDs in a stress-free GaAs/ZnSe/QD–Ge/ZnSe system. The distinctive properties of this system are a small mismatch of the lattice parameters (~0.2%), a high density of QDs (up to 10^{12} cm^{-2}), and high values of the energy barrier for both electrons and holes. As was shown in [6], for structures with Ge QDs arranged between ZnSe layers of equal thickness, Coulomb staircase-type features were observed at room temperature in the current–voltage (CV) characteristic, whereas spectral dependences of photovoltage in the growth direction indicated that the absorption occurs in the layer with QDs. The results obtained made it possible to construct a band diagram of the structure. From a consideration of this diagram, it became clear that, in the structure asymmetrical with respect to the ZnSe layer thickness, charge accumulation in the layer with QDs can proceed upon illumination by means of electron escape through tunneling into gallium arsenide. If such a layer is used as the floating gate in a field-effect transistor structure in which a thin epitaxial layer of germanium serves as the channel, it becomes possible to study the process of charge accumulation in the structure with Ge QDs. In this case, the accumulation of even a very small charge must lead to a measurable change in the channel current.

The goal of this work was to investigate the process of charge accumulation in a QD and to determine the characteristic relaxation times.

Transistor structures were fabricated by molecular beam epitaxy (MBE) and represented the following sequence of layers on an *n*+GaAs substrate. First, a SiO layer 0.4 μm thick was grown on a gallium arsenide wafer. Next, windows were opened in SiO with the use of photolithography, and ZnSe/QD–Ge/ZnSe/*p*-Ge structures were grown in these windows. The thickness of the first layer was ~15 nm, the thickness of the second layer was ~120–150 nm, and the thickness of the epitaxial single-crystal germanium film was 40 nm. The next process was metal deposition and the creation of aluminum contacts by photolithography. The distance between the aluminum contacts was 8 μm. Indium served as a contact to gallium arsenide. A schematic diagram of the structure is given in the inset in Fig. 1.

CV characteristic. The germanium channel current was measured at T = 300 and 77 K. Typical current–voltage characteristics in the dark are given in Fig. 1.

The transverse current through the structure is much lower than the longitudinal channel current, so that it cannot introduce any error into the measurements, whereas the current in the channel tends to saturate for both temperatures. In addition, it turned out that a decrease in the full current was observed upon illumination of the structure with white light on the side of the channel.

Dependence of the channel current on the incident radiation spectrum. The behavior of the structure upon illumination was investigated in detail by measuring the spectral dependences of the channel current at a constant signal with the use of a spectral KSVU-6 system. The measurements were performed at temperatures of 77 and 300 K with the voltage across the channel in the range 20–150 mV. The spectral dependence of the change in the full current in the germanium channel at a sweeping voltage of 50 mV is shown in Fig. 2. Light illumination with a wavelength shorter than 0.5 μm leads to a decrease in the current, and the current increases at longer wavelengths.

Current relaxation upon switching on and after switching off the illumination. Figure 3 presents relaxation curves of the channel current after switching off the illumination measured at room temperature for wavelengths of 0.6, 0.5, and 0.4 μm. The change of sign in the channel current observed upon illumination can in principle be associated with either the effect of the charge accumulated at one or another site of the structure on the channel conductivity, because the effect of the transverse current was excluded.

To determine the role of the QD on the photocurrent in the channel and its relaxation, structures were fabricated in which, instead of the layer with QDs, a layer of continuous material of the same thickness was grown. In such structures, the dependence of the current through the channel on the illumination was not observed. This fact testifies that the absorption in the layer with QDs is the decisive factor. The possible

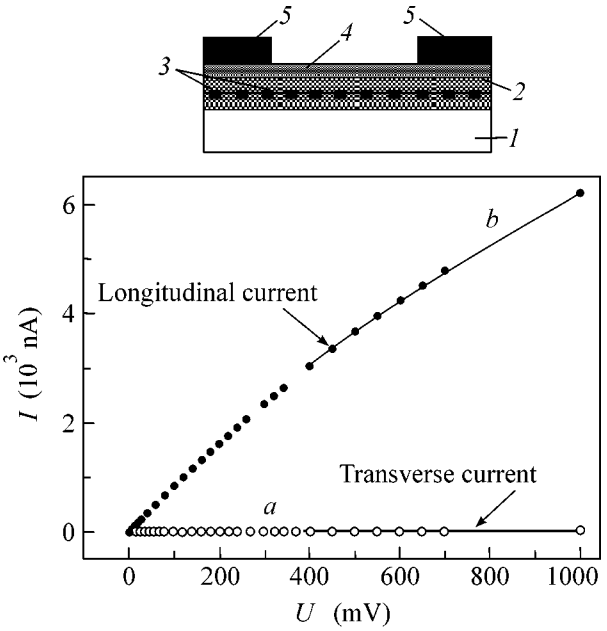

Fig. 1. CV characteristic and schematic diagram of the structure: (*a*) transverse and (*b*) longitudinal currents through the structure; (*1*) GaAs, (*2*) ZnSe, (*3*) QD–Ge, (*4*) *p*-Ge channel, and (*5*) Al contact. T = 300 K.

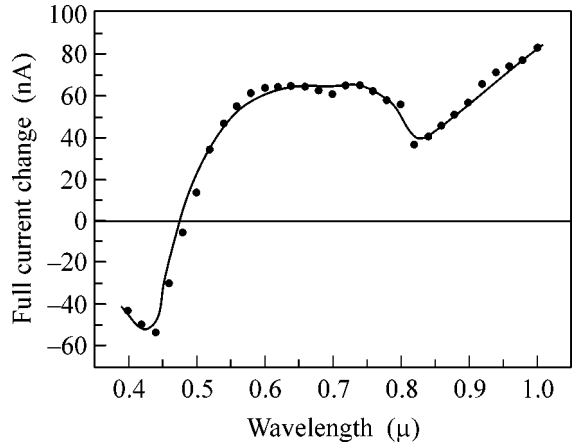

Fig. 2. Spectral dependence of the change in the full channel current.

mechanism of the decrease in the channel current upon illumination and the long-term current relaxation after switching off the illumination can be analyzed by considering the band diagram of the structure (Fig. 4) constructed based on the data on band discontinuities obtained in our previous work [6].

As a result of a calculation without the external voltage and illumination, it was found that the part of the built-in potential applied to germanium, the charge density on QDs, and the electron density on charged

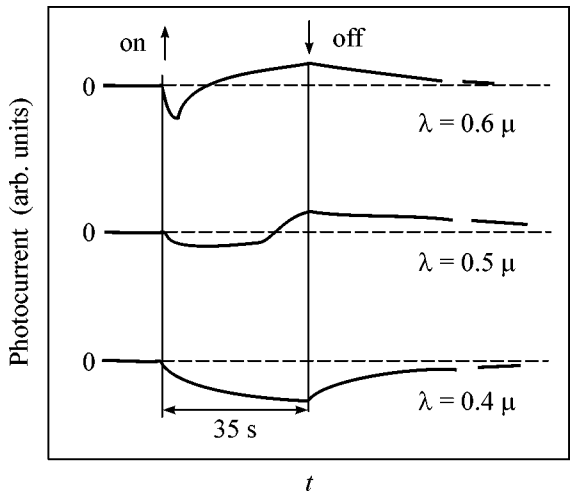

Fig. 3. Dependence of the channel current upon switching on and switching off illumination at different wavelengths, $T = 300$ K.

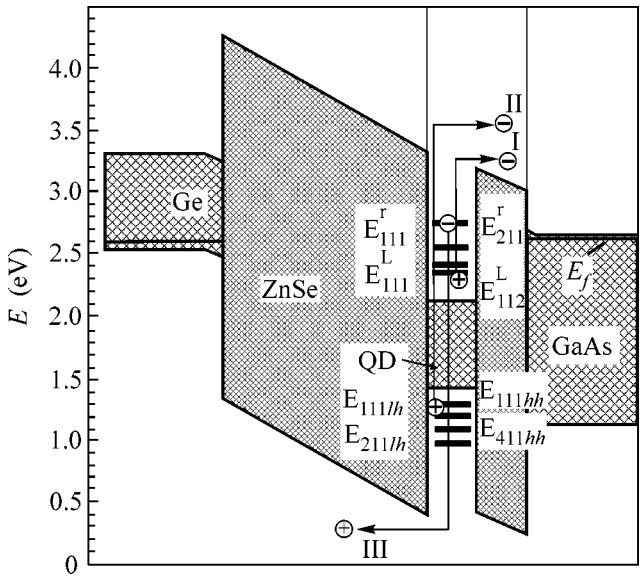

Fig. 4. Band diagram of the structure in equilibrium. Arrows show possible optical transitions followed by the escape of an electron (hole) and the localization of the second charge carrier. Only overbarrier transitions are shown, though tunneling into GaAs can also take place.

QDs were respectively as follows: $V_{Ge} = 0.033$ V, $\sigma_{QD} = -6.1 \times 10^{-8}$ C/cm^2, and $N_{eQD} = 3.8 \times 10^{11}$ cm^{-2}.

Because the transverse leakage currents through the structure are small, the channel current can be changed only through spatial localization of electrons and holes. Consider possible optical transitions in the structure (Fig. 4), starting from small photon energies. From the band diagram, it is evident that the transitions of type **I** from the conduction band levels lying below the Fermi level to the levels of the quasi-continuous spectrum can take place at $h\nu \geq 1.0$ eV, whereas the appearance of photocurrent in the experiment is observed at $h\nu \cong 1.25$ eV. For the transitions from the first valence band level to the levels from which electrons can tunnel into GaAs or to the levels of the quasi-continuous spectrum (transitions **II** in Fig. 4), the minimum quantum energy approximately equals 2.0–2.1 eV. Finally, for the transitions of electrons from the quasi-continuous spectrum of the valence band to the empty electron levels of QDs (transition **III** in Fig. 4), the minimum required energy is more than 2.3 eV.

How does charge localization proceed at these transitions? At transition **I**, an electron in the built-in electric field passes into gallium arsenide and a hole is localized on a QD. The same situation is observed for transition **II**. At the same time, at transitions **III**, an electron is localized in a QD and a hole passes into germanium (or is captured by a trap in ZnSe).

The charging of QDs with holes (transitions **I** and **II** in Fig. 4) must result in an increase in the transverse field and an inflow of electrons to the Ge–ZnSe heteroboundary; that is, a field effect must be observed. As the positive charge on QDs grows, depletion changes into inversion, which results in an increase in the channel conductivity and current and eventually leads to a steady state in which an increase in the current is observed. The dynamics of the variation of the channel conductivity as a function of the charge accumulation time is clearly demonstrated in Fig. 3 by the curves corresponding to the absorption of radiation with wavelengths of 0.6 and 0.5 μm. At photon energies starting from 2.3 eV, transitions of at least two types (**II** and **III**) can be observed; that is, QDs can be charged by both holes and electrons.

In this case, the channel current in the steady state will be determined by steady-state equilibrium between the generation and recombination processes of charge carriers of both signs and the process of their separation. In addition, at transitions of type **III**, the ejection of holes into the channel and the decrease of the transverse field in the channel prevent the attainment of the state of inversion. Therefore, if this type of excitation is accomplished in the experiment at $\lambda < 0.5$ μm, the depletion of the channel is observed, which results in a negative change in the current (Fig. 3). This is distinct from the case of $\lambda > 0.5$ μm, when transitions of only types **I** and **II** with the accumulation of a positive charge on QDs are observed.

The relaxation curves allow the characteristic times of the attainment of the steady state to be estimated. In this case, this is the state when generation is balanced by the recombination of electron–hole pairs and the fluxes of charge carriers from the QD–Ge layer there and back in both directions are equal to each other. These times range up to tens of seconds at room tem-

perature and grow to hours as the temperature decreases to 77 K.

An estimation of the charge that must be accumulated in QDs to reach the inversion point (the equality of the concentration of the minority carriers (electrons) to the concentration of holes) in the quasi-neutral bulk of the germanium channel indicates that $\sigma_{QD} = (4.2–4.7) \times 10^{-7}$ C/cm^2, which corresponds to the hole density on the charged QDs $N_{pQD} = (2.6–2.9) \times 10^{12}$ cm^{-2}.

Thus, the time dependences of the photocurrent at an incident light wavelength of 0.5 and 0.6 μm are associated with the gradual accumulation of holes in the QDs and must depend on the illumination intensity. At the same time, the steady state characterized by a decrease in the photocurrent upon excitation by light with a wavelength of 0.4 μm is associated with the appearance of transitions of another type. A more detailed analysis of absorption processes can be performed with known coefficients of light absorption in the QDs.

To conclude, it has been found experimentally that the transistor structure in the GaAs/ZnSe/QD–Ge/ZnSe/Ge system upon illumination by light differing in spectral composition exhibits variations of the channel current associated with the charging of QDs. Measurements of relaxation curves after switching off the illumination show that the decay of the current lasts for from tens of seconds to several hours, depending on the temperature of the object. The variations of the channel current indicated above have been explained with allowance made for the variation of the channel state near the heteroboundary from depletion to inversion. This effect can be used in long-term optical memory elements.

This work was supported by the Russian Foundation for Basic Research, project no. 02-02-17800, and by the programs Surface Atomic Structures and Low-Dimensional Quantum Structures.

REFERENCES

1. L. Guo, E. Leobundung, and S. Y. Chou, Science **275**, 649 (1997).
2. N. N. Ledentsov, V. M. Ustinov, V. A. Shchukin, *et al.*, Fiz. Tekh. Poluprovodn. (St. Petersburg) **32**, 385 (1998) [Semiconductors **32**, 343 (1998)].
3. M. Iwamatsu and Y. Okabe, J. Appl. Phys. **86**, 5541 (1999).
4. Y. W. Zhang, Phys. Rev. B **61**, 10388 (2000).
5. A. I. Yakimov, C. J. Adkins, R. Boucher, *et al.*, Phys. Rev. B **59**, 12598 (1999).
6. I. Yu. Borodin, I. A. Litvinova, I. G. Neizvestnyĭ, *et al.*, Pis'ma Zh. Éksp. Teor. Fiz. **78**, 184 (2003) [JETP Lett. **78**, 152 (2003)].

Translated by A. Bagatur'yants

JETP Letters, Vol. 78, No. 12, 2003, pp. 772–777. From Pis'ma v Zhurnal Éksperimental'noĭ i Teoreticheskoĭ Fiziki, Vol. 78, No. 12, 2003, pp. 1293–1298.

Topological Phase Separation in 2D Hard-Core Bose–Hubbard System Away from Half-Filling¶

A. S. Moskvin, I. G. Bostrem, and A. S. Ovchinnikov

Ural State University, Yekaterinburg, 620083 Russia

Received November 14, 2003

We suppose that the doping of the 2D hard-core boson system away from half-filling may result in the formation of a multicenter topological defect such as charge order (CO) bubble domain(s) with Bose superfluid (BS) and extra bosons both localized in domain wall(s), or a *topological* CO + BS *phase separation*, rather than a uniform mixed CO + BS supersolid phase. Starting from the classical model, we predict the properties of the respective quantum system. The long-wavelength behavior of the system is believed to resemble that of granular superconductors, CDW materials, Wigner crystals, and multiskyrmion system akin in a quantum Hall ferromagnetic state of a 2D electron gas. © *2003 MAIK "Nauka/Interperiodica".*

PACS numbers: 05.30.Jp

One of the fundamental hot debated problems in bosonic physics concerns the evolution of the charge ordered (CO) ground state of 2D hard-core Bose–Hubbard (BH) model (hc-BH) with a doping away from half-filling. Numerous model studies steadily confirmed the emergence of "supersolid" phases with simultaneous diagonal and off-diagonal long-range order, while Penrose and Onsager [1] were the first to show, as early as 1956, that supersolid phases do not occur.

The most recent quantum Monte Carlo (QMC) simulations [2–4] found two significant features of the 2D BH model with a screened Coulomb repulsion: the absence of supersolid phase at half-filling and a growing tendency to phase separation (CO + BS) upon doping away from half-filling. Moreover, Batrouni and Scalettar [2] studied quantum phase transitions in the ground state of the 2D hc-BH Hamiltonian and have shown numerically that, contrary to the generally held belief, the most commonly discussed "checkerboard" supersolid is thermodynamically unstable and phase separates into solid and superfluid phases. The physics of the CO + BS phase separation in BH model is associated with a rapid increase of the energy of a homogeneous CO state with doping away from half-filling due to a large "pseudospin-flip" energy cost. Hence, it appears to be energetically more favorable to "extract" extra bosons (holes) from the CO state and arrange them into finite clusters with a relatively small number of particles. Such a droplet scenario is believed to minimize the long-range Coulomb repulsion [5]. However, immediately there arise several questions. Whether a simple mean-field approximation (MFA) and classical continuum model can predict such a behavior. What is the detailed structure of the CO + BS phase separated state? What are the main factors governing the essential low-energy and long-wavelength physics? Is it possible to make use of simple toy models?

In this letter, we present a topological scenario of CO + BS phase separation in a 2D hc-BH model with intersite repulsion. The extra bosons/holes doped to a checkerboard CO phase of 2D boson system are believed to be confined in the ring-shaped domain wall of the skyrmion-like topological defect, which looks like a bubble domain in an easy-axis antiferromagnet. This allows us to propose the mechanism of 2D *topological* CO + BS *phase separation* when the doping of the bare checkerboard CO phase results in the formation of a multicenter topological defect, whose simplified pseudospin pattern looks like a system of bubble CO domains with Bose superfluid confined in charged ring-shaped domain walls.

The Hamiltonian of hard-core Bose gas on a lattice can be written in a standard form as follows:

$$H_{BG} = -\sum_{i>j} t_{ij}\hat{P}(B_i^\dagger B_j + B_j^\dagger B_i)\hat{P} + \sum_{i>j} V_{ij}N_iN_j - \mu\sum_i N_i, \quad (1)$$

where $\hat{P}$ is the projection operator which removes double occupancy of any site, $N_i = B_i^\dagger B_i$, and μ is the chemical potential determined from the condition of fixed full number of bosons $N_l = \sum_{i=1}^{N}\langle N_i\rangle$ or concentration $n = N_l/N \in [0, 1]$. The t_{ij} denotes an effective transfer integral, V_{ij} is an intersite interaction between the bosons. Here, $B^\dagger(B)$ are the Pauli creation (annihilation) operators which are Bose-like commuting for different

¶ This article was submitted by the authors in English.

sites $[B_i, B_j^\dagger] = 0$, for $i \neq j$, while for the same site $B_i^2 = (B_i^\dagger)^2 = 0$, $[B_i, B_i^\dagger] = 1 - 2N_i$, $N_i = B_i^\dagger B_i$; N is a full number of sites.

The model of hard-core Bose gas (BG) with an intersite repulsion is equivalent to a system of spins $s = 1/2$ exposed to an external magnetic field in the z-direction

$$H_{BG} = \sum_{i>j} J_{ij}^{xy}(s_i^+ s_j^- + s_j^+ s_i^-) + \sum_{i>j} J_{ij}^z s_i^z s_j^z - h\sum_i s_i^z, \quad (2)$$

where

$$J_{ij}^{xy} = 2t_{ij}, \quad J_{ij}^z = V_{ij}, \quad h = \mu - \sum_{j(j\neq i)} V_{ij}, \quad s^- = \frac{1}{\sqrt{2}}B,$$

$$s^+ = -\frac{1}{\sqrt{2}}B^\dagger, \quad s^z = -\frac{1}{2} + B_i^\dagger B_i, \quad s^\pm = \mp\frac{1}{\sqrt{2}}(s^x \pm is^y).$$

In frames of a conventional two-sublattice MFA approach, one may introduce two vectors, the ferromagnetic and antiferromagnetic ones:

$$\mathbf{m} = \frac{1}{2s}(\langle \mathbf{s}_1\rangle + \langle \mathbf{s}_2\rangle); \quad \mathbf{l} = \frac{1}{2s}(\langle \mathbf{s}_1\rangle - \langle \mathbf{s}_2\rangle);$$

$$\mathbf{m}^2 + \mathbf{l}^2 = 1,$$

where $\mathbf{m}\cdot\mathbf{l} = 0$. For the plane where these vectors lie, one may introduce two-parametric angular description: $m_x = \sin\alpha\cos\beta$, $m_z = -\sin\alpha\sin\beta$, $l_x = \cos\alpha\sin\beta$, $l_z = \cos\alpha\cos\beta$. The hard-core boson system in a two-sublattice approximation is described by two diagonal order parameters l_z and m_z and two complex off-diagonal order parameters $m_\pm = \mp\frac{1}{\sqrt{2}}(m_x \pm im_y)$ and $l_\pm = \mp\frac{1}{\sqrt{2}}(l_x \pm il_y)$. The complex superfluid order parameter $\Psi(\mathbf{r}) = |\Psi(\mathbf{r})|\exp - i\varphi$ is determined by the in-plane components of ferromagnetic vector: $\Psi(\mathbf{r}) = \frac{1}{2}\langle(\hat{B}_1 + \hat{B}_2)\rangle = sm_- = sm_\perp\exp - i\varphi$, $m_\perp$ being the length of the in-plane component of ferromagnetic vector. So, for a local condensate density, we get $n_s = s^2 m_\perp^2$. It is of interest to note that, in fact, all the conventional uniform $T = 0$ states with nonzero $\Psi(\mathbf{r})$ imply simultaneous long-range order for both modulus $|\Psi(\mathbf{r})|$ and phase φ. The in-plane components of antiferromagnetic vector $l_\pm$ describe a staggered off-diagonal order. It is worth noting that, by default, one usually considers the negative sign of the transfer integral t_{ij} that implies the ferromagnetic in-plane pseudospin ordering.

The model exhibits many fascinating quantum phases and phase transitions. Early investigations predict at $T = 0$ CO, BS, and mixed (CO + BS) supersolid uniform phases with an Ising-type melting transition (CO-NO) and Kosterlitz–Thouless-type (BS-NO) phase transitions to a nonordered normal fluid (NO) [6]. The detailed mean-field and spin-wave analysis of the uniform phases of 2D hc-BH model is given by Pich and Frey [7].

MFA yields, for the conventional uniform supersolid phase,

$$\sin^2\beta = m_z\frac{\sqrt{V-2t}}{\sqrt{V+2t}}; \quad \sin^2\alpha = m_z\frac{\sqrt{V+2t}}{\sqrt{V-2t}}$$

with a constant chemical potential $\mu = 4s\sqrt{(V^2 - 4t^2)}$. It should be noted that the supersolid phase appears to be unstable with regard to small perturbations in the Hamiltonian. The mean-field energy per site of the uniform supersolid phase is written as follows [7]:

$$E_{SS} = E_{CO} + s\mu m_z = E_{CO} + \mu\left(n_B - \frac{1}{2}\right),$$

where $E_{CO} = -2Vs^2$. The cost of doping for both CO and CO + BS phase appears to be rather high as compared with an easy-plane BS phase at half-filling, where the chemical potential turns into zero [8].

Magnetic analogy allows us to make unambiguous predictions as regards the doping of BH system away from half-filling. Indeed, the boson/hole doping of checkerboard CO phase corresponds to the magnetization of an antiferromagnet in z direction. In the uniform easy-axis l_z phase of anisotropic antiferromagnet, the local spin-flip energy cost is rather big. In other words, the energy cost for boson/hole doping into checkerboard CO phase appears to be big due to a large contribution of boson–boson repulsion.

However, the magnetization of the anisotropic antiferromagnet in an easy axis direction may proceed as a first-order phase transition with a "topological phase separation" due to the existence of antiphase domains [9]. The antiphase domain walls provide the natural nucleation centers for a spin-flop phase having enhanced magnetic susceptibility as compared with small, if any, longitudinal susceptibility, thus providing the advantage of the field energy. Namely, domain walls would specify the inhomogeneous magnetization pattern for such an anisotropic easy-axis antiferromagnet in relatively weak external magnetic field. As concerns the domain type in quasi-two-dimensional antiferromagnet, one should emphasize the specific role played by the cylindrical or bubble domains, which have finite energy and size. These topological solitons have the vortexlike in-plane spin structure and often named "skyrmions." The classical, or Belavin–Polyakov (BP), skyrmion [10] describes the solutions of a nonlinear σ-model with a classical isotropic 2D

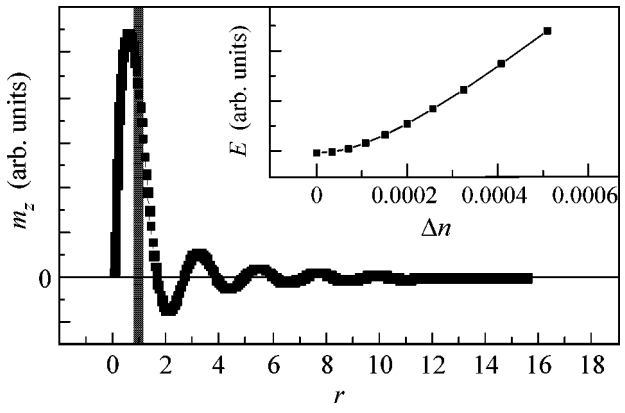

The results of numerical calculations by shooting method for a shrunk skyrmion given $v = 2.1$, $t = 1$: main panel—the radial distribution of the order parameter m_z (the filled region points to a center of a domain wall); the inset shows the dependence of the soliton energy on the number Δn of bosons bound in a domain wall.

Heisenberg Hamiltonian and represents one of the generic toy model spin textures. It is of primary importance to note that skyrmion-like bubble domains in easy-axis layered antiferromagnets were actually observed in the experiments performed by Waldner [11], which were supported later by different authors (see, e.g., [12, 13]). Although some questions were not completely clarified and remain open until now [14, 15], the classical and quantum [16] skyrmion-like topological defects are believed to be a genuine element of essential physics of both ferro- and antiferromagnetic 2D easy-axis systems.

The magnetic analogy seems to be a little bit naive; however, it catches the essential physics of doping the hc-BH system. As regards the checkerboard CO phase of such a system, namely a finite energy skyrmion-like bubble domain [17] seems to be the most preferable candidate for the domain with antiphase domain wall providing the natural reservoir for extra bosons. The classical description of nonlinear excitations in hc-BH model includes the skyrmionic solution given $V = 2t$ [17]. The skyrmion spin texture consists of a vortexlike arrangement of the in-plane components of ferromagnetic **m** vector with the l_z component reversed in the center of the skyrmion and gradually increasing to match the homogeneous background at infinity. The simplest spin distribution within a classical skyrmion is given as follows:

$$m_x = m_\perp \cos(\varphi + \varphi_0); \quad m_y = m_\perp \sin(\varphi + \varphi_0);$$
$$m_\perp = \frac{2r\lambda}{r^2 + \lambda^2}; \quad l_z = \frac{r^2 - \lambda^2}{r^2 + \lambda^2}, \tag{3}$$

where φ_0 is a global phase ($U(1)$ order parameter) and λ is the skyrmion radius. The skyrmion spin texture describes the coexistence and competition of the charge order parameter l_z and BS order parameter $m_\perp$, which reflects a complex spatial interplay of potential and kinetic energies. The skyrmion looks like a bubble domain in an easy-axis magnet. Skyrmions are characterized by the magnitude and sign of its topological charge, by its size (radius), and by the global orientation of the spin. The scale invariance of classical BP skyrmionic solution reflects in that its energy does not depend on radius and global phase. An interesting example of topological inhomogeneity is provided by a multicenter BP skyrmion [10] whose energy does not depend on the position of the centers. The latter are believed to be addressed as an additional degree of freedom or positional order parameter.

It should be noted that the domain wall in such a bubble domain somehow created in the checkerboard CO phase of 2D hc-BH system represents an effective ring-shaped reservoir for both Bose superfluid and extra boson/hole. Indeed, the magnetic response of a fixed radius skyrmion to a weak longitudinal external magnetic field can be approximated as follows:

$$m_z(r) \approx \chi(r) h,$$

where $\chi(r) = f(r) m_\perp(r)$ is a local magnetic susceptibility and $f(r)$ has distinct maximum at the domain wall center $r = \lambda$ with oscillating behavior $f(r) \propto J_1(r\sqrt{2}) \propto \sin(r\sqrt{2} + \pi/4)/\sqrt{r}$ for large r. The oscillating character of the magnetization distribution seems to reflect a skyrmion instability. Thus, we conclude that the extra boson/hole density described by the order parameter m_z is to be localized in the domain wall. This result is supported by numerical calculations for the static skyrmion-like excitations in a continuous 2D hc-BH model with a strong boson–boson repulsion, which was considered by us earlier in [17]. The figure sketches the calculated radial distribution of the order parameter m_z for a single bubble domain in hc-BH system with injected small boson concentration away from half-filling. It appears to be trapped inside the domain wall. As expected, the soliton energy depends quadratically on the number Δn of bosons bound in the domain wall (see inset in the figure), similarly to that of homogeneous BS phase [8]. In other words, $\partial E/\partial n = 0$ and one might say about a zero value of the effective boson/hole chemical potential for the CO bubble domain configuration would it be a ground state.

In the continuous model, the classical BP skyrmion is a topological excitation and cannot dissipate. However, according to the Hobart–Derrick theorem [18], the static solitons in two-dimensional easy-axis magnets are unstable to collapse. The classical static skyrmion is unstable with regard to an external field, anisotropic interactions of both easy-plane and easy-axis type. Small easy-axis anisotropy or external field are sufficient to shrink skyrmion to a nanoscopic size when magnetic length l_0,

$$l_0 = \left(\sqrt{(2V/t)^2 - (\mu/t)^2} - 4\right)^{-1/2}$$

is of the order of several lattice parameters and the continuous approximation fails to correctly describe excitations. Nonetheless, Abanov and Pokrovsky [19] have shown that the easy-axis anisotropy together with fourth-order exchange term can stabilize skyrmion with radius $R \propto \sqrt{l_0}$.

A skyrmionic scenario in hc-BH model allows us to make several important predictions. Away from half-filling, one may anticipate the nucleation of a topological defect in the unconventional form of the multicenter skyrmion-like object with ring-shaped Bose superfluid regions positioned in an antiphase domain wall separating the CO core and CO outside of the single skyrmion. The specific spatial separation of BS and CO order parameters that avoid each other reflects the competition of kinetic and potential energy. Such a *topological* (CO + BS) *phase separation* is believed to provide a minimization of the total energy as compared with its uniform supersolid counterpart. Thus, the parent checkerboard CO phase may gradually lose its stability under boson/hole doping, while a novel topological self-organized texture is believed to become stable. The most probable possibility is that every domain wall accumulates a single boson or boson hole. Then, the number of centers in a multicenter skyrmion nucleated with doping has to be equal to the number of bosons/holes. In such a case, we anticipate the near-linear dependence of the total BS volume fraction on the doping. Generally speaking, one may assume a scenario when the nucleation of a multicenter skyrmion occurs spontaneously with no doping. In such a case, we should anticipate the existence of a neutral multicenter skyrmion-like object with equal number of positively and negatively charged single skyrmions. However, in practice, namely the boson/hole doping is likely to be a physically clear driving force for a nucleation of a single or multicenter skyrmionlike self-organized collective mode in the form of multicenter charged topological defect, which may be (not strictly correctly) referred to as multiskyrmion system akin in a quantum Hall ferromagnetic state of a two-dimensional electron gas [20]. In such a case, we may characterize an individual skyrmion by its position (i.e., the center of skyrmionic texture), its size (i.e., the radius of domain wall), and the orientation of the in-plane components of pseudospin ($U(1)$ degree of freedom). An isolated skyrmion is described by the inhomogeneous distribution of the CO parameter, or staggered boson density l_z, order parameter m_z characterizing the deviation from the half-filling, and $m_\perp$ that corresponds only to the modulus of the superfluid order parameter.

It seems likely that, for a light doping, any doped particle (boson/holes) results in a nucleation of a new single-skyrmion state; hence, its density changes gradually with particle doping. Therefore, as long as the separation between skyrmionic centers is sufficiently large, so that the interskyrmion interaction is negligible, the energy of the system per particle remains almost constant. This means that the chemical potential of boson or hole remains unchanged with doping and, hence, apparently remains fixed.

The multiskyrmionic system, in contrast with uniform ones, can form the structures with inhomogeneous long-range ordering of the modulus of the superfluid order parameter accompanied by the unordered global phases of single skyrmions. Such a situation resembles in part that of granular superconductivity.

In the long-wavelength limit, the off-diagonal ordering can be described by an effective Hamiltonian in terms of $U(1)$ (phase) degree of freedom associated with each skyrmion. Such a Hamiltonian contains a repulsive, long-range Coulomb part and a short-range contribution related to the phase degree of freedom. The latter term can be written out in the standard for the *XY* model form of a so-called Josephson coupling

$$H_J = -\sum_{\langle i,j\rangle} J_{ij}\cos(\varphi_i - \varphi_j), \tag{4}$$

where φ_i and φ_j are global phases for skyrmions centered at points i and j, respectively, and J_{ij} is the Josephson coupling parameter. Namely, the Josephson coupling gives rise to the long-range ordering of the phase of the superfluid order parameter in a multicenter skyrmion. Such a Hamiltonian represents a starting point for the analysis of disordered superconductors, granular superconductivity, insulator–superconductor transition with $\langle i, j\rangle$ array of superconducting islands with phases φ_i, φ_j. Calculating the phase-dependent part of skyrmion–skyrmion interaction, Timm *et al.* [21] arrived at *negative* sign of J_{ij}, which favors antiparallel alignment of the $U(1)$ pseudospins. In other words, two skyrmions are assumed to form a peculiar Josephson π microjunction. There are a number of interesting implications that follow directly from this result [22]: the spontaneous breaking of time-reversal symmetry with nonzero supercurrents and magnetic fluxes in the ground state, long-time tails in the dynamics of the system, unconventional Aharonov–Bohm period $hc/4e$, and negative magnetoresistance.

To account for Coulomb interaction and allow for quantum corrections, we should introduce into effective Hamiltonian the charging energy [22]

$$H_{\rm ch} = -\frac{1}{2}q^2\sum_{i,j} n_i (C^{-1})_{ij} n_j,$$

where n_i is a boson number operator for bosons bound in ith skyrmion; it is quantum-mechanically conjugated to φ: $n_i = -i\partial/\partial\varphi_i$, $(C^{-1})_{ij}$ stands for the capacitance matrix, q for bosonic charge.

Such a system appears to reveal a tremendously rich quantum-critical structure. In the absence of disorder, the $T = 0$ phase diagram of the multiskyrmion system implies either triangular or square crystalline arrangements (Skyrmion crystal) with possible melting transition to a Skyrmion liquid. It should be noted that anal-

ogy with charged 2D Coulomb gas implies the Wigner crystallization of multicenter skyrmion with Wigner crystal (WC) to Wigner liquid melting transition, respectively. Naturally, the additional degrees of freedom for a skyrmion provide a richer physics of Skyrmion lattices. For a WC to be an insulator, disorder is required, which pins the WC and also causes the crystalline order to have a finite correlation length. The traditional approach to a Wigner crystallization implies the formation of a WC for densities lower than a critical density, when the Coulomb energy dominates over the kinetic energy. The effect of quantum fluctuations leads to a (quantum) melting of the solid at high densities or at a critical lattice spacing. The critical properties of a two-dimensional lattice without any internal degree of freedom are successfully described applying the BKT theory to dislocations and disclinations of the lattice and proceeds in two steps. The first implies the transition to a liquid-crystal phase with short-range translational order, and the second, the transition to isotropic liquid. Disorder pins the Skyrmion lattice and also causes the crystalline order to have a finite correlation length. For such a system, provided the skyrmion positions fixed at all temperatures, the long-wavelength physics would be described by an antiferromagnetic *XY* model with expectable BKT transition and gapless *XY* spin-wave mode.

As regards the superfluid properties, the skyrmion liquid reveals unconventional behavior with two critical temperatures $T_{BS} \leq t$ and $T_c \leq J$, T_{BS} being the temperature of the ordering of the modulus and $T_c < T_{BS}$, that of the phase of order parameter Ψ.

The low-temperature physics in Skyrmion crystals is governed by an interplay of two BKT transitions, for the $U(1)$ phase and positional degrees of freedom, respectively [21]. Dislocations in most Skyrmion lattice types lead to a mismatch in the $U(1)$ degree of freedom, which makes the dislocations bind fractional vortices and lead to a coupling of translational and phase excitations. Both BKT temperatures either coincide (square lattice), or the melting one is higher (triangular lattice) [21].

Quantum fluctuations can substantially affect these results. Quantum melting can destroy the $U(1)$ order at sufficiently low densities where the Josephson coupling becomes exponentially small. A similar situation is expected to take place in the vicinity of structural transitions in Skyrmion crystal. With increasing the skyrmion density, the quantum effects result in a significant lowering of the melting temperature as compared with classical square-root dependence. The resulting melting temperature can reveal an oscillating behavior as a function of particle density with zeros at the critical (magic) densities associated with structural phase transitions.

In terms of our model, the positional order corresponds to an incommensurate charge density wave, while the $U(1)$ order corresponds to superconductivity. In other words, we arrive at a subtle interplay between two orders. The superconducting state evolves from a charge order with $T_C \leq T_m$, where T_m is the temperature of a melting transition which could be termed as a temperature of the opening of the insulating gap (pseudogap!?).

The normal modes of a dilute skyrmion system (multicenter skyrmion) include the pseudospin waves propagating in between the skyrmions, the positional fluctuations, or phonon modes of the skyrmions, which are gapless in a pure system but gapped when the lattice is pinned, and, finally, fluctuations in the skyrmionic in-plane orientation and size. The last two types of fluctuation are intimately connected, since the z component of spin and orientation are conjugate coordinates because of commutation relations of quantum angular momentum operators. So, rotating a skyrmion changes its size. The orientational fluctuations of the multiskyrmion system are governed by the gapless *XY* model [20]. The relevant model description is most familiar as an effective theory of the Josephson junction array. An important feature of the model is that it displays a quantum-critical point.

The low-energy collective excitations of skyrmion liquid include a usual longitudinal acoustic phonon branch. The liquid crystal phases differ from the isotropic liquid in that they have massive topological excitations, i.e., the disclinations. One should note that the liquids do not support transverse modes; these could survive in a liquid state only as overdamped modes. So, it is reasonable to assume that solidification of the skyrmion lattice would be accompanied by a stabilization of transverse modes with its sharpening below melting transition. In other words, an instability of transverse phonon modes signals the onset of melting.

A generic property of the positionally ordered skyrmion configuration is the sliding mode, which is usually pinned by the disorder. The depinning of sliding mode(s) can be detected in a low-frequency and low-temperature optical response.

In conclusion, the boson/hole doping of the hard-core boson system away from half-filling is assumed to be a driving force for a nucleation of a multicenter skyrmion-like self-organized collective mode that resembles a system of CO bubble domains with a Bose superfluid and extra bosons both confined in domain walls. Such a *topological* CO + BS *phase separation*, rather than a uniform mixed CO + BS supersolid phase, is believed to describe the evolution of hc-BH model away from half-filling. Starting from the classical model, we predict the properties of the respective quantum system. In frames of our scenario, we may anticipate for the hc-BH model the emergence of an inhomogeneous BS condensate for superhigh temperatures $T_{TPS} \leq t$ and 3D superconductivity for rather high temperatures $T_c \leq J < t$. The system is believed to reveal many properties typical of granular superconductors, CDW materials, Wigner crystals, and multiskyrmion

system akin in a quantum Hall ferromagnetic state of a 2D electron gas. Topological inhomogeneity is believed to be a generic property of 2D hard-core boson systems away from half-filling.

Despite all the shortcomings, MFA and continuous approximation are expected to provide a physically clear semiquantitative picture of the rather complex transformations taking place in bare CO system with doping and can be instructive as a starting point to analyze possible scenarios. First of all, the MFA analysis allows us to consider the antiphase domain wall in CO phase to be a very efficient ring-shaped potential well for the localization of a single extra boson (hole), thus forming a novel type of topological defect with a single-charged domain wall. Such a defect can be addressed as a charged skyrmion-like quasiparticle whose energy can be approximated by its classical value for a CO bubble domain. It is of great importance to note that the domain wall simultaneously represents a ring-shaped reservoir for Bose superfluid.

Unfortunately, we have no experience to deal with multicenter skyrmions as regards its structure, energetics, and stability. It should be noted that such a texture with strongly polarizable centers is believed to provide an effective screening of long-range boson–boson repulsion, thus resulting in an additional self-stabilization. Nucleation of topological phase is likely to proceed in the way typical for the first-order phase transitions. The present paper establishes only the framework for analyzing the subtleties of the phase separation in a lattice hc-BH model away from half-filling. Much work remains to be done in both macroscopic and microscopic approaches.

ACKNOWLEDGMENTS

We acknowledge the support by SMWK grant, INTAS (grant no. 01-0654), CRDF (grant no. REC-005), RME (grant nos. E 02-3.4-392 and UR.01.01.042), and the Russian Foundation for Basic Research (grant no. 01-02-96404). One of us (A.S.M.) has benefited from discussions with C. Timm, S.-L. Drechsler, and T. Mishonov.

REFERENCES

1. O. Penrose and L. Onsager, Phys. Rev. **104**, 576 (1956).
2. G. G. Batrouni and R. T. Scalettar, Phys. Rev. Lett. **84**, 1599 (2000).
3. F. Hébert, G. G. Batrouni, R. T. Scalettar, *et al.*, Phys. Rev. B **65**, 014513 (2001).
4. G. Schmid, S. Todo, M. Troyer, and A. Dorneich, Phys. Rev. Lett. **88**, 167208 (2002).
5. M. Yu. Kagan, K. I. Kugel, and D. I. Khomskiĭ, Zh. Éksp. Teor. Fiz. **120**, 470 (2001) [JETP **93**, 415 (2001)].
6. R. T. Scalettar, G. G. Batrouni, A. P. Kampf, and G. T. Zimanyi, Phys. Rev. B **51**, 8467 (1995).
7. Ch. Pich and E. Frey, Phys. Rev. B **57**, 13712 (1998).
8. K. Bernardet, G. G. Batrouni, J.-L. Meunier, *et al.*, Phys. Rev. B **65**, 104519 (2002).
9. The antiferromagnetic domain texture appears as a result of the minimization of elastic and magnetoelastic energies.
10. A. A. Belavin and A. M. Polyakov, Pis'ma Zh. Éksp. Teor. Fiz. **22**, 503 (1975) [JETP Lett. **22**, 245 (1975)].
11. F. Waldner, J. Magn. Magn. Mater. **54–57**, 837 (1986); Phys. Rev. Lett. **65**, 1519 (1990).
12. S. I. Belov and B. I. Kochelaev, Solid State Commun. **103**, 249 (1997).
13. Carsten Timm and K. H. Bennemann, Phys. Rev. Lett. **84**, 4994 (2000).
14. T. Kamppeter, S. A. Leonel, F. G. Mertens, *et al.*, Eur. Phys. J. B **21**, 93 (2001).
15. D. D. Sheka, B. A. Ivanov, and G. Mertens, Phys. Rev. B **64**, 024432 (2001).
16. R. A. Istomin and A. S. Moskvin, JETP Lett. **71**, 338 (2000).
17. A. S. Ovchinnikov, I. G. Bostrem, and A. S. Moskvin, Phys. Rev. B **66**, 134304 (2002).
18. R. H. Hobart, Proc. Phys. Soc. London **82**, 201 (1963); G. H. Derrick, J. Math. Phys. **5**, 1252 (1964).
19. Ar. Abanov and V. L. Pokrovsky, Phys. Rev. B **58**, R8889 (1998).
20. A. G. Green, Phys. Rev. B **61**, R16299 (2000).
21. Carsten Timm, S. M. Girvin, and H. A. Fertig, Phys. Rev. B **58**, 10634 (1998).
22. S. A. Kivelson and B. Z. Spivak, Phys. Rev. B **45**, 10490 (1992).

JETP Letters, Vol. 78, No. 12, 2003, pp. 778–779. Translated from Pis'ma v Zhurnal Éksperimental'noĭ i Teoreticheskoĭ Fiziki, Vol. 78, No. 12, 2003, pp. 1299–1300.

In Memory of Our Contributors

PACS numbers: 01.60.+q

S. N. Ermolov *et al.*, "Superconducting MgB_2 Films Obtained by Magnetron Sputtering," 73, 557 (2001)

Sergeĭ Nikolaevich Ermolov died suddenly of a heart attack on December 27, 2001. He was born in 1956 in Voronezh. After graduation from the Department of Solid-State Physics of the Faculty of Physics of Voronezh State University in 1979, he was engaged as a junior research assistant at the Institute of Solid-State Physics (ISSP) of the USSR Academy of Sciences. From 1986, after successfully defending his Candidate Dissertation at the ISSP, Dr. Ermolov worked as a research assistant at the Institute of Problems of Microelectronics of the USSR Academy of Sciences. In 1990, he took a job at the Gorizont Experimental Design Bureau as a senior research assistant, pursuing experimental studies at the ISSP, where he returned in 1995 already as a senior research assistant.

A death is always a tragedy, but a premature death of a scientist who is full of pith and brimful of ideas is perceived as a huge tragedy that cannot be understood and accepted. S.N. Ermolov was a highly qualified specialist in both the electronic and magnetic properties of thin films of low- and high-temperature superconductors and the technology of their production. He will remain in our memory as a distinguished experimentalist who developed a number of original procedures for obtaining thin epitaxial films of high-T_c superconductors by magnetron and laser sputtering. Sergeĭ Nikolaevich was always at the frontline of the physics of superconductors of both cuprates and new compounds. His results on nonstoichiometric BaNbO films published in Phys. Rev. B and on MgB_2 films reported in his last work published recently in JETP Letters are of most interest.

In recent years, Dr. Ermolov was fascinated with a new scientific problem associated with studying surface atomic layers of single-crystal materials. The main subjects of his investigations were metals with a bulk-centered lattice and high melting points, such as W, Mo, Ta, etc., used as matrix elements in cathode structures. In his investigations, Sergeĭ Nikolaevich successfully employed a set of modern methods that included low-energy ion scattering, low-energy electron diffraction, Auger electron spectrometry, quadrupole mass spectrometry, work-function measurements, etc. Dr. Ermolov obtained single crystals for his investigations using original growth techniques. The main problems that were solved in these investigations were in understanding the mechanisms of ion back scattering, neutralization, and charge exchange at the surface of single-crystal samples doped with barium, rhenium, and other elements to decrease the work function. The results of these studies were published in Phys. Rev. B and other recognized scientific journals.

All that was done by Sergeĭ Nikolaevich in his short life will remain in his colleagues' hearts as cherished memory of this remarkable man and scientist.

I. I. Kogan *et al.*, "Feigenbaum Universality in String Theory," 77, 260 (2003)

A well-known theoretical physicist Ian Il'ich Kogan died suddenly on June 4, 2003, at the age of 44. Ian Il'ich passed away at the very height of his power and creative activities. The breadth of Ian Il'ich's interests was extraordinary. These included quantum chromodynamics, supersymmetry and supergravitation, string theory, conformal field theory, condensed media, D-branes and cosmology, quantum gravitation, etc. It is difficult to cite everything. In all these areas, he obtained important results.

Ian Il'ich discovered and investigated phase transitions in string theory; he was one of the authors of logarithmic conformal field theories and multigravitation theory and actively studied the application of methods of conformal field theory and string theory in solid-state theory. His scientific productivity was also extraordinary: Dr. Kogan was the author of about 200 works and had 60 coauthors; he had followers at the Institute of Experimental and Theoretical Physics and at Oxford University, where Ian Il'ich worked as a professor for the last ten years.

The world scientific community bewails the departure of the eminent scientist and man.

A. N. Oraevsky, "Is There a Collective Dielectric Resonance?" 78, 5 (2003)

Anatoliĭ Nikolaevich Oraevsky, doctor of physics and mathematics, professor, the Lenin Prize winner, an eminent physicist working in the field of masers and lasers, quantum optics, and interaction of laser radiation with matter, died suddenly on July 4, 2003.

0021-3640/03/7812-0778$24.00

A.N. Oraevskiĭ was the author of more than 450 research works, 200 inventions, and 5 monographs; his fundamental works on the dynamics of lasers and other nonlinear optical systems, quantum frequency standards, laser chemistry, and chemical lasers gained international recognition.

About 40 years Anatoliĭ Nikolaevich worked as a professor at the Moscow Institute of Engineering Physics, where he delivered an original course of lectures on quantum radiophysics. More than 40 degree works and 32 candidate dissertations were defended under his supervision; 10 of his followers became doctors of science.

Anatoliĭ Nikolaevich was not only an eminent scientist. A delightful companion, a man with a remarkable sense of humor whose scope of knowledge seemed sometimes just a marvel, Anatoliĭ Nikolaevich was a genuine intellectual and gentleman who possessed traditional habitudes of kindliness and courtesy and was always ready to come to the aid of somebody. A man of inquiring mind, encyclopedic knowledge, and the highest moral principles, he possessed a keen sense of justice, remained objective in any discussion, and was a rather exacting, but invariably well-intentioned referee and an understanding and rightful supervisor. It is impossible to be reconciled to his untimely departure, which is a grievous loss to all his friends and colleagues.

E. A. Shapoval, "Boundary Conditions to the Ginzburg–Landau Equations at the Twinning Plane in a (d+s) Superconductor," 76, 579 (2002)

Zhenya Shapoval entered the third year of the Physical Faculty of Moscow State University in the fall of 1954. From the very first studies, his high scientific abilities became evident, which was recognized in full measure by our best teachers. His abilities were noticed by L.D. Landau, who taught statistical physics at that time, and later, quantum mechanics. Shapoval was the only one from our group who successfully passed the famous theoretical minimum already in 1958, the year of graduation from the University.

Zhenya did not restrict himself to purely professional activities. His delicate literary and musical sensibility and nontrivial judgments on painting reflected not simply his broad humanitarian education: an impression of his personal belonging to world culture. All this put together created an image of an extremely interesting and attractive person. He immediately cut a figure by clearly defined individual democratic outlook and by the boldness of his principle-based judgments in combination with deep decency and a noble code of honor.

By L.P. Gor'kov's suggestion, E.A. Shapoval developed a quasi-classical method for calculating the phenomenological coefficients of the Ginzburg–Landau theory. Based on the Shapoval method, the concept of diffuse scattering from the boundary between a superconductor and a normal metal, insulator, or ferromagnetic metal was formulated.

This method found wide use for calculating critical fields and critical currents and also for determining boundary conditions to the differential equations of superconductivity for both diffuse and mirror scattering from the boundary. Recently, this method has been used for high-T_c superconductors with *d*-pairing.

He loved science and continued to work despite all the tribulations of his rugged life. We all feel deeply sorry for Evgeniĭ Aleksandrovich!

Translated by A. Bagatur'yants